CAPITAL UNIVERSITY OF SCIENCE AND TECHNOLOGY, ISLAMABAD

In Silico Analysis of Bioactive Compounds from *Berberis vulgaris* Targeting *E6* and *E7* Oncoprotein of Human Papillomavirus Type 16: A Computational Approach to Antiviral Drug Discovery

by

Nimra Pervaiz

A thesis submitted in partial fulfillment for the degree of Master of Science

in the

Faculty of Health and Life Sciences
Department of Bioinformatics and Biosciences

2025

I dedicate this thesis to my loving mother and supportive family who have fully helped me in achieving my life goals.

CERTIFICATE OF APPROVAL

In Silico Analysis of Bioactive Compounds from *Berberis vulgaris* Targeting *E6* and *E7* Oncoprotein of Human Papillomavirus Type 16: A Computational Approach to Antiviral Drug Discovery

by

Nimra Pervaiz

(MBS241004)

THESIS EXAMINING COMMITTEE

S. No.	Examiner	Name	Organization
(a)	External Examiner	Dr. Rehana Rani	NUST, Islamabad
(b)	Internal Examiner	Dr. M. Asad Anwar	CUST, Islamabad
(c)	Supervisor	Dr. Erum Dilshad	CUST, Islamabad

Dr. Erum Dilshad
Thesis Supervisor
September, 2025

Dr. Syeda Marriam Bakhtiar
Head
Dept. of Bioinfo. & Biosciences
September, 2025

Dr. Sahar Fazal
Dean
Faculty of Health & Life Sciences
September, 2025

Author's Declaration

I, **Nimra Pervaiz** hereby state that my MS thesis titled "***In Silico* Analysis of Bioactive Compounds from *Berberis vulgaris* Targeting *E6* and *E7* Oncoprotein of Human Papillomavirus Type 16: A Computational Approach to Antiviral Drug Discovery**" is my own work and has not been submitted previously by me for taking any degree from Capital University of Science and Technology, Islamabad or anywhere else in the country/abroad.

At any time if my statement is found to be incorrect even after my graduation, the University has the right to withdraw my MS Degree.

(Nimra Pervaiz)

Registration No: MBS241004

Plagiarism Undertaking

I solemnly declare that research work presented in this thesis titled "***In Silico* Analysis of Bioactive Compounds from *Berberis vulgaris* Targeting *E6* and *E7* Oncoprotein of Human Papillomavirus Type 16: A Computational Approach to Antiviral Drug Discovery**" is solely my research work with no significant contribution from any other person. Small contribution/help wherever taken has been duly acknowledged and that complete thesis has been written by me.

I understand the zero tolerance policy of the HEC and Capital University of Science and Technology towards plagiarism. Therefore, I as an author of the above titled thesis declare that no portion of my thesis has been plagiarized and any material used as reference is properly referred/cited.

I undertake that if I am found guilty of any formal plagiarism in the above titled thesis even after award of MS Degree, the University reserves the right to withdraw/revoke my MS degree and that HEC and the University have the right to publish my name on the HEC/University website on which names of students are placed who submitted plagiarized work.

(Nimra Pervaiz)

Registration No: MBS241004

Acknowledgement

All praise and thanks to the Allah Almighty to whom we only bow down. I would also like to express my gratitude to my family especially my Mother for their continuous mental and physical support and prayers. I would also wholeheartedly say a big thank you to my supervisor Dr. Erum Dilshad (Associate Professor, Department of Bioinformatics and Biosciences, CUST) for her support for giving his precious time to assist with computational approaches.

(Nimra Pervaiz)

Abstract

Human Papillomavirus (HPV), particularly high-risk type 16, is a primary causative agent of cervical and other anogenital cancers. Despite the availability of preventive vaccines, no specific antiviral therapy currently exists to eliminate persistent HPV infections. The viral oncoproteins *E6* and *E7* play critical roles in disrupting tumor suppressor pathways, promoting uncontrolled cell proliferation and malignant transformation. The present study aims to explore the antiviral potential of Berberine and related bioactive compounds from *Berberis vulgaris* against HPV16 by targeting *E6* and *E7* oncoproteins using an *in silico* approach. FASTA sequences of *E6* and *E7* proteins were retrieved from UniProt and used for 3D structure prediction through SWISS-MODEL. Physicochemical properties and functional domains were analyzed using tools like ExPASy ProtParam and InterProScan. A set of 15 bioactive ligands from *Berberis vulgaris* were selected from PubChem, prepared using Chem3D Ultra, and subjected to energy minimization. Their drug-likeness and toxicity were assessed through Lipinski's Rule of Five and pkCSM, respectively. Molecular docking was performed using CB-Dock2, where several compounds, including Oxyacanthine, Coptisine, Thalifendine, and Jatrorrhizine, showed promising binding affinities with both *E6* and *E7* proteins. Among them, Thalifendine and Jatrorrhizine were identified as the most effective lead compounds based on optimal binding scores, ADME profiles, and non-toxic predictions. Their interactions were further visualized using PyMOL and analyzed with LigPlot+ to confirm hydrogen bonding and hydrophobic contacts within the active sites. Additionally, the lead compounds were compared with the FDA-approved antiviral agent Imiquimod, revealing comparable docking scores and superior safety profiles *in silico*. The findings suggest that berberine derivatives, particularly Thalifendine and Jatrorrhizine, hold potential as natural antiviral candidates against HPV16 and merit further in vitro and in vivo investigation for therapeutic development.

Keywords: *Berberis vulgaris* Human Papillomavirus (HPV), *In silico* analysis, *E6* and *E7* oncoproteins , Phytochemicals, ADMET profiling

Contents

List of Figures

List of Tables

Abbreviations

ADME	Absorption ,Distribution, Metabloism Excretion
DNA	Deoxyribonucleic Acid
FASTA	Fast Alignment Search Tool Algorithm
GRAVY	Grand Average of Hydropathy
HPV	Human Papillomavirus
HSPGs	Heparan Sulfate Proteoglycans

Chapter 1

Introduction

Viruses still represent a serious risk global health due to their rapid mutation rates and ability to evade immune responses, resulting in persistent infections and malignancies [1]. Among these, the Human Papillomavirus (HPV) is regarded as one of the most studied oncogenic viruses because of its strong connection with cervical cancer and other anogenital and oropharyngeal malignancies [2]. HPV is a small, double-stranded DNA virus that belonging to the Papillomaviridae family, comprising more than 200 identified types. so far [3]. Among various genotypes, HPV type 16 (HPV-16) has been identified as among the riskiest oncogenic types, responsible an estimated 50-60% of global cervical cancer cases [4, 5]. The oncogenic activity of HPV-16 primarily results from the actions of its early proteins E6 and E7. E6 leads to the breakdown of the tumor-suppressing protein p53, whereas E7 disables the retinoblastoma (pRb) protein, interfering with normal cell cycle control and encouraging uncontrolled cell growth, genomic instability, and eventually cancerous changes [6, 7]. Due to the critical role of E6 and E7 in HPV-mediated carcinogenesis, these viral oncoproteins are considered valuable molecular targets for antiviral drug development and therapeutic intervention [8] .In recent years, natural products have gained significant attention in drug discovery because of their structural diversity, lower toxicity, and wide pharmacological activities [9].

Berberis vulgaris (commonly known as barberry), is a widely used medicinal plant rich in alkaloids such as berberine, palmatine, jatrorrhizine, columbamine, and others, which demonstrate a wide range of pharmacological properties including anticancer, antiviral, antioxidant, and anti-inflammatory activities [9, 10].

The advancement of computational methods has facilitated *in silico* techniques like molecular docking, virtual screening, and molecular dynamics simulations for drug discovery.

These methods provide a cost-effective and time-saving strategy for identifying potential drug candidates by predicting binding interactions between target proteins and bioactive compounds [11, 12].

Therefore, in this study, an *in silico* investigation was conducted to analyze berberine and related bioactive compounds from Berberis Vulagris for their potential inhibitory activity targeting the E6 and E7 oncoproteins of HPV-16.

Molecular docking and computational approaches were used to evaluate the binding affinities and interaction profiles of these bioactive compounds as potential therapeutic agents against HPV-16 infections.

1.1 Problem Statement

Human Papillomavirus (HPV) play a significant role in the development of cerival cancer and various other malignancies, affecting millions worldwide. Current treatment strategies, including vaccines and antiviral medications, have limitations like high costs, limited accessibility, and inefficacy against existing infections. Medicinal plants offer a rich source of bioactive compounds with antiviral properties, but their potential against HPV remains largely unexplored. Computational (*in silico*) approaches, including molecular docking and dynamics simulations, provide a cost-effective and efficient method to screen and identify plant-derived compounds with strong binding affinity against HPV oncoproteins (E6 and E7). This study aims to utilize *in silico* techniques to identify potent plant-based inhibitors, offering a foundation for future drug development.

1.2 Aims and Objective

Aim:

To investigate bioactive compounds from *Berberis Vulgaris* through computational approaches for their potential inhibitory activity against HPV oncoproteins.

Objective:

The purposes of the study include:

a) To determine probable inhibitory compounds with antiviral properties present in *Berberis vulgaris* against HPV oncoproteins(E6 and E7) through molecular docking studies.

b) To analyze the interaction between ligand and protein complex by performing molecular docking.

c) To find the best of the interacting molecules that shows inhibitory effects against the virus.

1.3 Scope

This study will contribute to HPV treatment by identifying novel plant-based inhibitors using cost-effective computational tools. It will support the development of plant-derived antiviral agents, especially in regions with limited access to synthetic drugs. The research will highlight locally available medicinal plants, promoting their use in pharmaceutical applications. The findings will support the development of future within a living organism and outside the living body validation, paving the way for HPV-targeted herbal drug development.

Chapter 2

Literature Review

2.1 Human Papillomavirus(HPV)

Human Papillomavirus (HPV) is one of the most prevalent STI infections worldwide, responsible for a significant burden of cervical and other cancers [13].A non enveloped DNA virus with a double-standed genome, classified within the papillomaviridae family [14]. Over 200 genotypes of HPV was detected, which are categorized into high- risk and low risk groups according to their cancer-causing potential [15]. Among these, HPV-16 is the most prevalent high-risk type and has been closely linked to cervical cancer development, accounting for nearly 50-60% of cases worldwide [16, 17]. The primary mechanism through which HPV-16 contributes to carcinogenesis involves the Ongoing production of the viral oncoprotein *E6* and *E7* [18]. These oncoproteins target the host's tumor suppressor proteins (p53 and pRb), leading to uncontrolled cellular proliferation,mutation in the genome, and ultimately tumorigenic conversion [19, 20]. The figure 2.1 shows the structure of human Papillomavirus.The virus is composed of capsid made of protein subunits,which encases its circular double-standed DNA genome.The outer capsid is responsible for protecting the genetic material and facilitating viral entry into host cell [19].

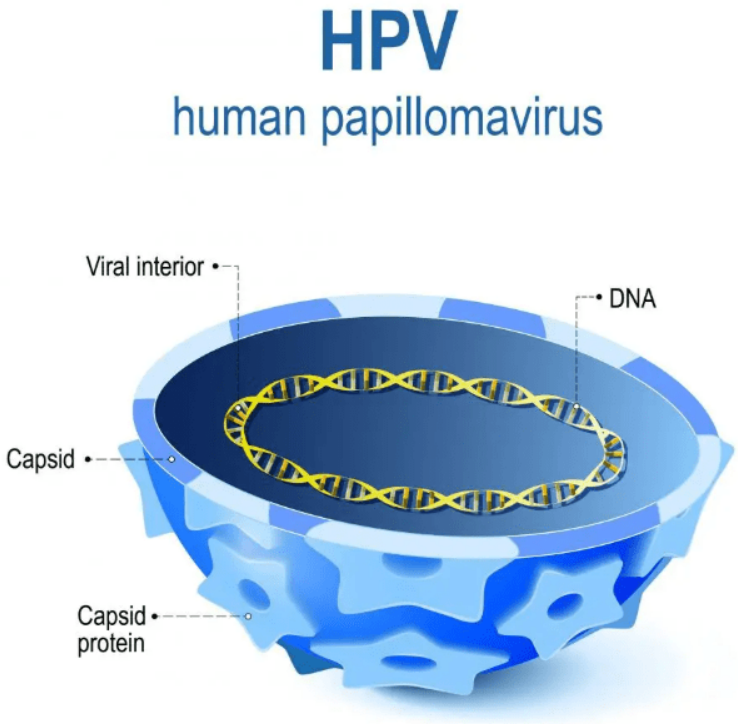

FIGURE 2.1: Structure of Human Papillomavirus [19]

2.2 Origin

Human Papillomavirus (HPV) is an ancient virus that has mutually evolved with its vertebrate hosts for millions of years. The origin of papillomaviruses is believed to date back more than 300 million years, possibly coinciding with the early evolution of amniotes (reptiles, birds, and mammals) [21]. Genetic studies suggest that papillomaviruses have undergone host-specific evolution, resulting in their wide diversity and adaptation to specific species over time [22]. HPVs members of the papillomaviridae family, characterized by small, non-enveloped, double-stranded DNA viruses. These viruses infect the squamous epithelium of the skin and mucosal surfaces of their hosts, leading to benign or malignant lesions based on viral type and host factors [23]. The extensive diversity of HPV types is thought to have resulted from long-term co-divergence with host species combined with more recent host-switching events and intra-host viral diversification [24]. This evolutionary history explains the existence of more than 200 distinct HPV genotypes identified to date, many of which exhibit strong species and tissue tropism [25].

2.3 Entry and Life Cycle

Human Papillomavirus (HPV) initiates infection through microabrasions or minor injuries in the epithelial tissue, which expose the basal layer of keratinocytes—the primary target cells of the virus [26]. The virus first adheres to the host cells by heparan sulfate proteoglycans (HSPGs) binding situated on the basement membrane or the matrix outside the cell . This initial binding triggers conformational changes in the viral capsid that expose sites for cleavage by host enzymes such as furin, allowing subsequent interactions with secondary cellular receptors including integrins, tetraspanins (e.g., CD151), and growth factor receptors [27, 28]. These interactions facilitate the internalization of HPV through clathrin-dependent or clathrin-independent endocytosis, depending on the HPV genotype and host cell type[29]. Following internalization, the virus traffics through the endosomal system, where the minor capsid protein L2 be essential in protecting the viral genome and mediating escape from the endosomes. L2 escorts the viral DNA to the trans-Golgi network, ensuring the genome is safely transported within the host cell while avoiding degradation by host defenses [30]. As the infected basal cells progress through mitosis, the nuclear envelope temporarily disassembles, allowing the L2-genome complex to enter the nucleus [31]. Once inside the nucleus, the viral DNA exists as an episome and establishes a persistent infection in the host cell. The replication within the viral genome this stage is supported by viral proteins E1 and E2, which coordinate viral DNA replication and maintenance at low copy numbers within dividing cells [32].

During the differentiation and upward migration of infected basal cells towards the epithelial surface,the virus undergoes replication and produces new viral particles activates its late gene expression program. In these terminally differentiated cells, the viral genome undergoes extensive replication, and the structural proteins L1 and L2 are expressed to form new viral capsids [33]. Virion assembly occurs in the nucleus, and mature viral particles accumulate in the upper epithelial layers. Eventually, new virions are released into the environment as the superficial epithelial cells are naturally shed, completing the viral life cycle without causing cell lysis or triggering strong immune responses, which helps HPV evade host immune

surveillance and establish persistent infections [34, 35]. Figure 2.2 illustrates the life cycle of Human Papillomavirus (HPV) within epithelial tissues. The virus initially attaches to the basal epithelial cells through micro-abrasions in the skin or mucosa. After entry, it utilizes the host cell machinery for replication and begins a regulated program of gene expression as the infected cell moves upward through the layers of the epithelium. In the upper layers, late gene expression and capsid formation occur, leading to the assembly of new viral particles. These mature virions are then released from the surface without cell lysis, enabling the virus to spread while evading immune detection[35].

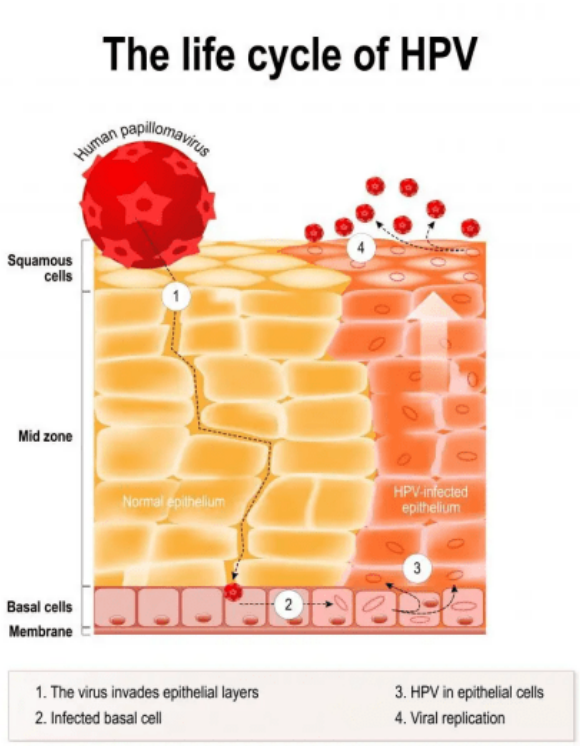

FIGURE 2.2: The life cycle of HPV [35]

2.4 Symptoms of Human Papillomavirus (HPV) Infection

Human Papillomavirus (HPV) infections are typically asymptomatic in most individuals, particularly during the early stages of infection [36]. In many cases, individuals may carry the virus for months or years without showing any clinical

symptoms, and the infection may resolve spontaneously due to the host immune response [37]. However,Persistent infection, particularly with high-risk HPV strains like HPV-16 and HPV-18, can result in the emergence of various precancerous and cancerous lesions depending on the anatomical location [38]. The most common clinical manifestation of Low-risk HPV types, including HPV-6 and HPV-11, typically cause benign genital warts (condyloma acuminata), which appear in the genital and perianal regions. These lesions are usually soft, flesh-colored, and can vary in size and number [39]. Low-risk HPV types may also cause oral papillomas, laryngeal papillomatosis, and conjunctival papillomas [40]. In contrast,High-risk strains, especially HPV-16 and HPV-18, are closely linked with the onset of precancerous conditions and multiple cancers such as cervical, vulvar, vaginal, anal, penile, and oropharyngeal cancers. [41].In cervical infections, persistent HPV can alter cervical epithelial cells, causing cervical intraepithelial neoplasia (CIN), which may progress to invasive cervical cancer if not treated.[42]. Early-stage cervical lesions are usually asymptomatic, but advanced stages may present with abnormal vaginal bleeding, pelvic pain, or dyspareunia (pain during intercourse) [43]. Oral HPV infections, often caused by HPV-16, may lead to oropharyngeal cancers involving the tonsils, tongue base, and throat. Symptoms may include sore throat, difficulty swallowing, hoarseness, and neck swelling [44]. In rare cases, recurrent respiratory papillomatosis (RRP) can occur when HPV infects the respiratory tract, causing wart-like growths in the larynx and airways, leading to voice changes and breathing difficulties [45]. Overall, the clinical presentation of HPV infection varies widely depending on the viral type, site of infection, duration of persistence, and the host's immune status. Regular screening programs, such as Pap smear tests and HPV DNA testing, are crucial for early detection and prevention of HPV-associated malignancies, especially cervical cancer [46].

2.5 HPV Statistics in Pakistan

In Pakistan, Human Papillomavirus (HPV) poses a serious public health challenge, primarily due to its strong link with cervical cancer, which is identified as the third

most frequently occurring cancer among women and the second leading cancer in females aged 15 to 44 years[47]. Each year, approximately 5,000–5,600 new cervical cancer cases are reported, leading to 3,000 - 3,900 deaths annually [48, 49].

Studies show that high-risk HPV types, particularly HPV-16 and HPV-18, are responsible for about 88% of invasive cervical cancer cases in Pakistan [50]. Several regional studies have reported HPV DNA detection several regional studies have reported HPV DNA detection in 85–95% of cervical cancer tissues, with HPV-16 being the most dominant genotype, followed by HPV-18 and other high-risk types such as HPV-45 and HPV-31 [51, 52].

Despite this burden, HPV screening programs remain limited, and HPV vaccine coverage is extremely low due to lack of awareness, cost barriers, and absence of a national vaccination program [53].

Recent efforts are ongoing to introduce HPV vaccination into public health programs; however, as of now, routine screening and vaccination remain largely unavailable across the country [54, 55].

2.6 Treatment for Human Papillomavirus (HPV)

Currently, there is no direct antiviral therapy accessible eradicate Human Papillomavirus (HPV) infections directly; instead, management focuses on treating HPV-related lesions and preventing progression to malignancy.

For low-risk HPV types causing genital warts, topical agents such as imiquimod, podophyllotoxin, and trichloroacetic acid, as well as surgical methods like cryotherapy, laser ablation, and excision, are commonly used [56].

In high-risk HPV infections associated with cervical intraepithelial neoplasia (CIN) and cervical cancer, treatment involves surgical excision procedures such as loop electrosurgical excision procedure (LEEP), cold knife surgery, or hysterectomy depending on the severity of the lesions [57].

Preventive measures, including HPV vaccination (e.g., Gardasil and Cervarix), are essential in decreasing incidence of new infections and cervical cancer cases; however, therapeutic vaccines and direct antiviral agents targeting HPV oncoproteins *E6* and *E7* are still under investigation and not yet available for clinical use [58].

2.7 Medicinal Plants in HPV

Medicinal plants have been widely explored as a potential source of antiviral compounds due to their chemical diversity, low toxicity, and broad pharmacological properties. Several plant-derived compounds have demonstrated activity against Human Papillomavirus (HPV) infections, particularly by targeting viral replication, immune modulation, and inhibition of the viral oncoproteins *E6* and *E7*, which play central roles in HPV-induced carcinogenesis [59]. Natural compounds such as flavonoids, alkaloids, terpenoids, and polyphenols exhibit antiviral, antioxidant, anti-inflammatory, and anticancer effects, making them promising candidates for complementary or alternative HPV therapies [60]. Among these, *Berberis vulgaris* and its major bioactive compounds have attracted considerable attention due to their strong anticancer and antiviral activities. Most of Bioactive compounds has been reported to suppress HPV oncogene expression, induce apoptosis, and inhibit the proliferation of HPV-infected cervical cancer cells by modulating key cellular pathways such as p53 and NF-κB signaling [61, 62]. In vitro studies have shown that bioactive compounds can downregulate the expression of *E6* and *E7* oncoproteins, thereby restoring the function of tumor suppressor proteins like p53 and pRb, which are crucial for cell cycle control and apoptosis [63]. Additionally, other medicinal plants such as Curcuma longa (curcumin), Camellia sinensis (epigallocatechin gallate), Resveratrol, and Withania somnifera (withaferin A) have also demonstrated inhibitory effects against HPV-induced cellular transformations through various molecular mechanisms, including inhibition of viral gene expression, suppression of inflammation, and induction of apoptosis in HPV-positive cells [64, 65]. These phytochemicals may serve as promising leads for the development of safe and effective antiviral agents targeting HPV

infections. While several medicinal plants have shown encouraging results in pre-clinical studies, most of these findings are limited to in vitro and animal models. Further clinical trials are necessary to validate their efficacy and safety in humans. Nevertheless, plants represent a valuable source of bioactive compounds that may contribute to future therapeutic strategies for HPV-associated diseases, especially in resource-limited settings where conventional therapies are less accessible [66].

2.8 Role of Bioactive Compounds in Targeting HPV

Some bioactive compounds, are natural isoquinoline alkaloid primarily isolated from *Berberis vulgaris*, has been widely studied for its broad pharmacological activities, including antiviral, anticancer, antimicrobial, anti-inflammatory, and antioxidant properties [67]. In recent years, increasing attention has been given to bioactive compounds potential role in inhibiting Human Papillomavirus (HPV) infection and its associated oncogenic effects, particularly through modulation of the viral oncoproteins *E6* and *E7*, which are critical for HPV-induced carcinogenesis [68, 69]. One of the primary mechanisms by which bioactive compounds exerts its antiviral activity against HPV is through the downregulation of *E6* and *E7* gene expression. By suppressing these viral oncogenes, bioactive compounds helps restore the normal function of tumor suppressor proteins such as p53 and retinoblastoma protein (pRb), which are normally inactivated by HPV infection [70]. The reactivation of these tumor suppressor pathways promotes cell cycle arrest, apoptosis, and inhibition of abnormal cell proliferation, ultimately reducing the malignant transformation of infected cells [71]. In addition to its direct effects on viral gene expression, bioactive compounds has also been shown to interfere with several cellular signaling pathways involved in HPV-mediated tumor progression. Studies have reported that bioactive compounds suppresses the activity of transcription factors such as NF-κB and AP-1, both of which are involved in promoting the expression of HPV oncogenes and supporting inflammation and cellular transformation [72]. Furthermore, bioactive compounds may exert epigenetic

effects by modulating histone acetylation, further contributing to the suppression of HPV oncogene transcription [73]. Several in a laboratory studies using HPV-positive cervical cancer cell lines (e.g., HeLa and SiHa) have demonstrated that bioactive compounds treatment results in significant reduction in cell growth induction of apoptosis, and reduction in HPV *E6/E7* expression levels [74]. These findings imply that bioactive compounds may serve as a promising natural compound for the development of novel therapeutic agents targeting HPV infection and HPV-induced cancers. While current evidence from preclinical studies is encouraging, clinical studies evaluating the effectiveness of bioactive compounds in treating HPV infections and associated cancers are still limited. Further research, including clinical trials, is necessary to establish bioactive compounds therapeutic potential, optimal dosing, and safety profile in the context of HPV-related diseases [75]. This Fig 2.3 depicts *Berberis vulgaris*, commonly known as barberry, a medicinal shrub recognized for its small, oblong red berries and spiny branches. Widely distributed across Europe, Asia, and parts of North Africa, *Berberis vulgaris* has been traditionally used in herbal medicine due to its bioactive compounds which exhibits antimicrobial, antioxidant, and anticancer properties. The plant is studied extensively for its potential therapeutic applications, including use in treating infections, inflammation, and even metabolic disorders. Its relevance in modern pharmacology continues to grow as research explores its role in various drug development strategies.

FIGURE 2.3: *Berberis vulagris* [75]

2.9 Taxonomic Hierarchy of *Berberis vulgaris*

Berberis vulgaris is the binomial name of the plant belonging to the Berberidaceae family. The taxonomic classification of one of the primary sources of *Berberis vulgaris* (Common Barberry), is shown in Table 2.1 [75].

TABLE 2.1: Taxonomic hierarchy of *Berberis vulgaris* [75]

Sr.	Category	Value
1.	Kingdom	Plantae
2.	Sub kingdom	Viridiplantae
3.	Infra kingdom	Streptophyta
4.	Superdivision	Embryophyta
5.	Division (Phylum)	Tracheophyta
6.	Subdivision	Spermatophytina
7.	Class	Magnoliopsida
8.	Order	Ranunculales
9.	Family	Berberidaceae
10.	Genus	Berberis
11.	Species	*Berberis vulgaris* L.

2.10 Molecular Docking

Computational binding analysis is a widely used computational technique in drug design based on molecular structure that predicts the binding orientation and interaction of a small molecule with its target macromolecule (receptor or protein) [76]. This method helps to estimate the binding affinity, stability, and possible interaction mechanisms between ligands and their target proteins, thus providing important insights into the potential efficacy of candidate molecules before performing laboratory experiments [77]. The principle of molecular docking relies on the concept of "lock and key" or "induced fit", where the ligand fits into the active or binding site of the receptor protein in a stable and energetically favorable manner [78]. During the docking process, different poses (orientations) of the ligand are generated, and scoring functions are applied to evaluate the strength of

binding based on various parameters such as hydrogen bonding, hydrophobic interactions, electrostatic interactions, van der Waals forces, and binding free energy [79]. Molecular docking consists of two main steps: pose prediction (sampling) and scoring. In the sampling phase, the docking algorithm generates multiple ligand conformations and positions within the binding site of the protein. In the scoring phase, each pose is evaluated, and the best one is selected based on its predicted binding energy and interaction profile [80]. Lower binding energy values generally indicate stronger and more stable interactions between ligand and receptor [81] .In antiviral drug discovery, molecular docking is a valuable tool for identifying potential inhibitors of viral proteins by virtually screening large libraries of natural or synthetic compounds [82].

In the present study, molecular docking was employed to predict the association affinities of disease-fighting molecules from *Berberis vulgaris*, including berberine and related alkaloids, against the *E6* and *E7* oncoproteins of Human Papillomavirus type 16 (HPV-16).

The docking analysis allowed for the identification of potential linkage between the selected phytochemicals and also the functional area of the target proteins, providing preliminary insights into their possible antiviral activity [83]. The use of molecular docking in this study not only reduces time and cost compared to traditional wet-lab experiments but also helps to prioritize promising bioactive compounds for further experimental validation [84].

2.11 Bioactive Compounds as Inhibitors

Bioactive compounds, particularly those derived from medicinal plants, have emerged as promising inhibitors against various viral and cancer-related targets due to their structural diversity and ability to modulate multiple biological pathways.

These compounds can interfere with viral replication, suppress oncogene expression, and restore tumor suppressor activity by targeting specific proteins involved in disease progression. In the context of HPV, several phytochemicals such as

berberine, curcumin, epigallocatechin gallate, and resveratrol have demonstrated inhibitory effects on the *E6* and *E7* oncoproteins, thereby reactivating p53 and retinoblastoma pathways, inducing apoptosis, and inhibiting cellular proliferation. Their multitargeted mechanisms, combined with lower toxicity profiles, make bioactive compounds attractive candidates for developing safer and more effective therapeutic options against HPV-associated malignancies [83, 84].

2.12 Inhibitors Against Human Papillomavirus (HPV)

Several inhibitors have been explored to target Human Papillomavirus (HPV), particularly focusing on its two major oncoproteins, *E6* and *E7*, which play a critical role in carcinogenesis by disrupting the p53 and pRb tumor suppressor pathways. Small molecule inhibitors, natural compounds, siRNAs, and therapeutic vaccines have been investigated for their potential to block the activity or expression of these oncoproteins. Among natural inhibitors, compounds such as berberine, curcumin, epigallocatechin gallate, and resveratrol have shown promising results in downregulating *E6*/*E7* expression, reactivating tumor suppressor proteins, inducing apoptosis, and inhibiting the proliferation of HPV-infected cells. Although no specific FDA-approved antiviral agents directly targeting HPV oncoproteins exist yet, ongoing research on these inhibitors offers potential future therapeutic strategies for treating HPV-associated malignancies [84, 85].

Chapter 3

Methodology

FIGURE 3.1: Overview of Methodology

3.1 Selection of Disease

Human Papillomavirus (HPV) infection was chosen as the target disease for this study because of its powerful association with cervical cancer, a major cause of cancer-related deaths among women globally. Among the various genotypes, HPV type 16 (HPV-16) is the most prevalent high-risk strain, responsible for roughly 50-60% of all cervical cancer cases. The ongoing expression of two crucial oncoproteins, *E6* and *E7*, in HPV-16-infected cells plays a pivotal role in disrupting tumor suppressor pathways, resulting in unchecked cell growth and cancerous transformation. Taking into account the worldwide burden, shortage of healing treatments, and the primary role of *E6* and *E7* in HPV-induced cancer development, this study concentrates on HPV-16 as a target disease model to determine possible blockers from organic sources that may aid in medicinal advancement.

3.2 Selection of Protein

In this study, the *E6* and *E7* oncoproteins of Human Papillomavirus type 16 (HPV-16) were selected as the target proteins due to their critical role in viral-mediated oncogenesis. These proteins are consistently expressed in HPV-infected cells and are responsible for inactivating key tumor suppressor proteins such as p53 and retinoblastoma protein (pRb), leading to abnormal cell proliferation and malignant transformation. Their unique and essential function in the survival of HPV-infected cancer cells makes them ideal molecular targets for therapeutic intervention. Therefore, *E6* and *E7* proteins were selected for molecular docking analysis to evaluate their interactions with bioactive compounds derived from *Berberis vulgaris*.

3.3 Physical and Chemical Properties of Protein

The physical and chemical properties of the selected target proteins, *E6* and *E7* from HPV-16, were analyzed to understand their basic molecular characteristics,

which are essential for evaluating their stability and suitability for molecular docking. These properties include molecular weight, theoretical isoelectric point (pI), amino acid composition, instability index, aliphatic index, and grand average of hydropathicity (GRAVY). Such parameters provide insight into the solubility, hydrophobicity, and thermal stability of the proteins. The analysis was performed using the ProtParam tool available on the ExPASy server by submitting the FASTA sequences of the *E6* and *E7* proteins. The results showed that both proteins are small in size, with relatively high instability indices and varying hydropathic behavior, reflecting their flexible structure and interaction potential with small-molecule ligands during docking analysis.

3.4 Cleaning a Downloaded Protein

The 3D structures of the target proteins, *E6* and *E7* of HPV-16, were cleaned and prepared for molecular docking using PyMOL, a molecular visualization and editing tool. The downloaded protein structures in PDB format were opened in PyMOL to manually inspect and refine the models. Non-essential components such as water molecules (HOH), heteroatoms (HETATM), ligands, and additional chains were removed using PyMOL's command-line functions and graphical interface. After cleaning, the structure was visually checked for missing atoms, and the protein was saved in cleaned PDB format for further processing. This step ensured that only the relevant protein structure remained, allowing for more accurate binding site prediction and molecular docking results. The cleaned protein files were then used in the subsequent ligand docking workflow.

3.5 Target Protein Functional Domains Determination

To identify the biologically active and functionally important regions of the selected target proteins (*E6* and *E7* of HPV-16), their functional domains were

predicted using the NCBI Conserved Domain Database (CDD) and InterProScan. The amino acid sequences of both proteins in FASTA format were submitted to these online tools to analyze conserved motifs, binding sites, and characteristic structural domains. The analysis provided insights into the presence of conserved zinc-binding domains in *E6* and pRb-binding domains in *E7*, which are critical for their interaction with host cell tumor suppressor proteins such as p53 and pRb. Identifying these domains was essential for confirming the potential binding sites for ligand docking and ensuring that the selected compounds would interact with regions crucial to the protein's oncogenic activity. The domain information was further used to guide molecular docking, focusing on regions most likely to yield biologically relevant interactions.

3.6 Selection of an Active Metabolic Ligand

In this study, the selection of active metabolic ligands was based on phytochemical compounds naturally occurring in *Berberis vulgaris*, a medicinal plant known for its antiviral, anticancer, and antimicrobial properties. Bioactive alkaloids such as berberine, palmatine, jatrorrhizine, columbamine, and berbamine were shortlisted from literature and public chemical databases such as PubChem based on their reported pharmacological relevance. Structural data for each compound were retrieved from PubChem in .SDF or .PDB format, and only those molecules with drug-like characteristics (e.g., acceptable molecular weight, hydrogen bond donors/acceptors, and logP) were selected for further docking analysis. These ligands were expected to bind and potentially inhibit the functional domains of HPV-16 *E6* and *E7* oncoproteins, thus interfering with their oncogenic activities.

3.7 Ligand Preparation

The selected bioactive compounds from *Berberis vulgaris* were prepared for molecular docking through a standard ligand optimization process. The 3D structures

of the ligands were retrieved from the PubChem database in .SDF or .PDB format.The selected bioactive compounds from *Berberis vulgaris* were initially retrieved from the PubChem database in .SDF format, which provides standardized 3D molecular structures.

These structures were then imported into Chem3D Ultra software for geometry optimization and energy minimization. Within Chem3D, each ligand was visually inspected, and hydrogen atoms were added where necessary to complete the structure. The ligands were then subjected to energy minimization using the MM2 force field, which helps achieve a low-energy, stable conformation by optimizing bond angles, torsions, and non-bonded interactions.

After minimization, the structures were saved in .PDB format for compatibility with molecular docking software. This preparation step ensured that the ligands maintained their bioactive conformations and were structurally optimized for accurate docking analysis with the target HPV-16 *E6* and *E7* proteins.

3.8 Molecular Docking

Molecular docking was utilized to assess the binding affinity and interaction of selected bioactive compounds from *Berberis vulgaris* with the *E6* and *E7* oncoproteins of HPV-16.

The docking process employed PyRx, a virtual screening tool that leverages AutoDosck Vina as the docking engine. Protein structures were prepared and energy-minimized, then loaded in .PDBQT format, while ligands were converted to .PDBQT format using Open-Babel.

A grid box was defined around the active site to enable flexible docking, and simulations were run using default parameters. Binding affinities were recorded in kcal/mol, and top-ranked poses were selected for further analysis. Post-docking visualization and interaction analysis were performed using Discovery Studio Visualizer and PyMOL to examine hydrogen bonding, hydrophobic interactions, and binding orientation.

3.9 Visualization of Docking Results via PyMOL

After molecular docking, the best ligand–protein complexes, based on binding affinity scores, were selected for visualization and interaction analysis using PyMOL, a powerful molecular visualization software. The docked complexes in .PDBQT or .PDB format were opened in PyMOL to examine the spatial orientation of ligands within the binding site of the *E6* and *E7* proteins of HPV-16. Specific interactions such as hydrogen bonds, hydrophobic contacts, and π–π stacking were visually analyzed to evaluate the binding mode and compatibility of the ligand with the functional domain of the protein.

The ligand was displayed in stick representation, and the binding pocket residues were highlighted using surface or cartoon view for clarity. Screenshots of the docked complexes were captured for documentation and presentation in the Results section. This visualization helped to better interpret the molecular interaction between the bioactive compounds and target proteins and supported the selection of lead candidates for further *in silico* or experimental validation.

3.10 Analysis of a Docked Complex via LigPlot

To further evaluate and interpret the molecular interactions between the selected ligands and the target proteins (*E6* and *E7* of HPV-16), the docked complexes were analyzed using LigPlot+, a widely used tool for 2D visualization of protein–ligand interactions. The best docking poses, previously saved in .PDB format from PyRx or PyMOL, were imported into LigPlot+. The software automatically generated two-dimensional diagrams illustrating key non-covalent interactions, including hydrogen bonds (shown as dashed lines) and hydrophobic contacts (represented by spoked arcs). LigPlot+ also identified the specific amino acid residues involved in binding, helping to verify whether the ligands interacted within the functional domain of the proteins. This visual representation provided detailed insight into the binding mechanism and supported the rational selection of the most

promising bioactive compounds for further investigation. The 2D interaction diagrams were saved and documented for inclusion in the Results and Discussion sections.

3.11 Ligand ADME Properties

The ADME properties of the selected ligands were predicted using pkCSM, an online tool that applies graph-based signatures to evaluate pharmacokinetic behavior and drug-likeness of chemical compounds. The canonical SMILES of each bioactive compound from *Berberis vulgaris* were obtained from PubChem and submitted to the pkCSM web server. The tool generated predictive data for key pharmacokinetic parameters including intestinal absorption, blood–brain barrier (BBB) permeability, P-glycoprotein substrate or inhibitor status, cytochrome P450 enzyme interactions (especially CYP3A4 and CYP2D6), total clearance, and renal excretion. These parameters were used to assess the potential bioavailability, distribution, metabolism, and excretion profile of each ligand. Compounds showing acceptable ADME behavior were considered more suitable for further development as drug-like molecules targeting HPV-16 *E6* and *E7* proteins.

3.12 Lead Compound Identification

Following molecular docking, ADME analysis, and interaction visualization, the identification of lead compounds was carried out by selecting ligands that demonstrated the lowest binding energy, favorable binding interactions, and acceptable pharmacokinetic properties. Compounds from *Berberis vulgaris* were evaluated based on their docking scores against HPV-16 *E6* and *E7* oncoproteins, with a focus on those showing strong hydrogen bonding and hydrophobic interactions at key functional domains. Only those ligands that fulfilled both binding affinity and ADME criteria were considered as potential lead compounds. These lead candidates were prioritized for further consideration as potential therapeutic agents for

HPV-related malignancies, and their detailed docking poses and interaction profiles were documented for interpretation in the Results and Discussion sections.

3.13 Comparison with Standard Drug

Comparing a lead compound with a standard drug is crucial in drug discovery to evaluate its efficacy, safety, and pharmacokinetics. The comparison is based on several parameters, including binding affinity, ADME properties, toxicity, and therapeutic effectiveness. Binding Affinity: Molecular docking studies assess how well the lead compound binds to the target protein compared to a standard drug. Lower binding energy (ΔG) and stronger interactions indicate better potency. Pharmacokinetics (ADME): The lead compound is evaluated against the standard drug for absorption, distribution, metabolism, and excretion using tools like SwissADME and pkCSM. Higher bioavailability, better solubility, and lower toxicity are preferred. Toxicity Profile: The lead compound should have a better or comparable safety profile than the standard drug, assessed using *in silico* toxicity prediction (e.g., ProTox-II) and experimental assays. In Vitro and In Vivo Efficacy: Enzyme inhibition assays, cell-based studies, and animal models determine whether the lead compound shows similar or improved biological activity compared to the standard drug. Resistance and Selectivity: The lead compound should ideally show lower resistance development and higher target specificity, reducing off-target effects. A successful lead compound should demonstrate superior or comparable performance to the standard drug, making it a promising candidate for further optimization and clinical trials .

3.14 Drug Proposed Against Human Papilloma Virus

Several drugs have been proposed against Human Papillomavirus (HPV), targeting viral replication, immune response, and oncogene inhibition. Cidofovir, a

nucleotide analogue, disrupts HPV DNA replication, while Imiquimod, a TLR7 agonist, boosts immune response against HPV-infected cells. Therapeutic vaccines like VGX-31007 and ISA101 induce T-cell-mediated clearance of HPV-infected cells.Natural compounds such as Magnoflorine and Thalifendine inhibit HPV oncoproteins and restore apoptotic pathways. These therapeutic strategies hold promise for treating HPV-related diseases, including cervical cancer and genital warts.

Chapter 4

Results and Discussions

4.1 Structure Modelling

The *E6* and *E7* oncoproteins of Human Papillomavirus type 16 (HPV-16) were selected as the target proteins in this study to assess their interaction with major bioactive compounds present in *Berberis vulgaris*. This plant is known to contain various classes of natural compounds, including alkaloids (berberine, palmatine, jatrorrhizine, and berbamine), flavonoids , phenolic compounds, lignans , and terpenoids (oxycanthine, thalifendine). Among these, alkaloid-based molecules were primarily focused upon due to their previously reported antiviral and anticancer properties.

4.2 3D Structure of Protein

The complete 3D structures of HPV-16 *E6* and *E7* proteins were not available in the Protein Data Bank (PDB), so homology modeling was performed to predict their structure. The amino acid sequences of both proteins were obtained in FASTA format from the UniProt database. These sequences were submitted to the SWISS-MODEL online tool, which generated predicted structures based on available template proteins with similar sequences. The models were built using

automated comparative modeling techniques provided by the server. After generation, the predicted protein structures were downloaded in .pdb format and opened in PyMOL software to visualize the 3D arrangement. Important structural features like alpha-helices, beta-sheets, and loops were observed and show in figure 4.1 and figure 4.2. These modeled structures were further used for protein cleaning, domain identification, and molecular docking studies. The predicted models were found to be suitable for docking, as they showed proper folding and complete geometry for interaction with selected bioactive ligands.

FIGURE 4.1: Predicted 3D structure of HPV16 *E6* protein visualized in PyMOL

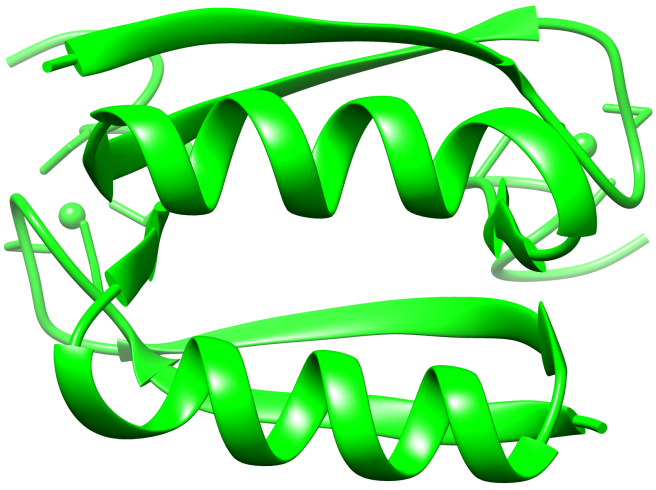

FIGURE 4.2: Predicted 3D structure of HPV16 *E7* protein visualized in PyMOL

4.3 Physical and Chemical Properties of Proteins

The basic physical and chemical properties of the modeled *E6* and *E7* oncoproteins of HPV-16 were analyzed using the ProtParam tool available on the ExPASy (Expert Protein Analysis System) server. The amino acid sequences in FASTA format were uploaded to calculate various molecular features. For the *E6* protein, the total number of amino acids was found to be (158), with a molecular weight of approximately (19187.28) kDa and a theoretical isoelectric point (pI) of (9.16) are show in Table 4.2 .Similarly, the *E7* protein consisted of 98 amino acids, with a molecular weight of around (11022.32)kDa and a theoretical pI of (4.20) are show in table 4.1.

Other important properties such as the aliphatic index, instability index, and grand average of hydropathicity (GRAVY) were also determined. These values provide insight into the stability, solubility, and hydrophilic/hydrophobic nature of the proteins. Both proteins showed suitable physicochemical profiles for further docking and interaction analysis, confirming that the predicted structures were reliable and appropriate for computational studies. With this, the protein showing pI greater than 7 means the basic nature of the protein whereas a pI value lesser than 7 indicates the acidic nature of the protein. Extinction coefficient indicates the light absorption whereas instability index represents stability level of protein if it is lesser than 40 then that means the protein is stable any value greater than 40 shows that protein is unstable [86].

TABLE 4.1: Physical properties of E7 protein

Properties	**Values**
Number of amino acids	98
Molecular weight	11022.32kDa
Total number of atoms	1499
Theoretical pI	4.2
Formula	$C_{469}H_{734}N_{124}O_{162}S_{10}$
Instability index	63.00(Unstable)

Table 4.1 continued from previous page

Properties	**Values**
Grand average of hydropathicity (GRAVY)	-0.405
Aliphatic index	78.57

TABLE 4.2: Physical properties of E6 protein

Properties	**Values**
Number of amino acids	158
Molecular weight	19187.28
Total number of atoms	9.16
Theoretical pI	$C_{835}H_{1327}N_{251}O_{235}S_{17}$
Formula	2665
Instability index	76.14 (Unstable)
Grand average of hydropathicity (GRAVY)	68.48
Aliphatic index	0.778

4.4 Identification of Active Region of a Protein

For identifying the functional domains InterPro consortium is used. InterPro helps in finding the functional analysis of proteins and classifies them into families which is done by finding functional domains and other important sites.

For identifying the functional domains InterPro consortium is used. InterPro helps in finding the functional analysis of proteins and classifies them into families which is done by finding functional domains and other important sites. Functional domains are the active part of the protein that is used by the protein for interacting with other proteins or other substances. Functional domains are the active part of the protein that is used by the protein for interacting with other proteins or other substances. In figure 4.3 and figure 4.4 illustrate the Functional domain of protein.

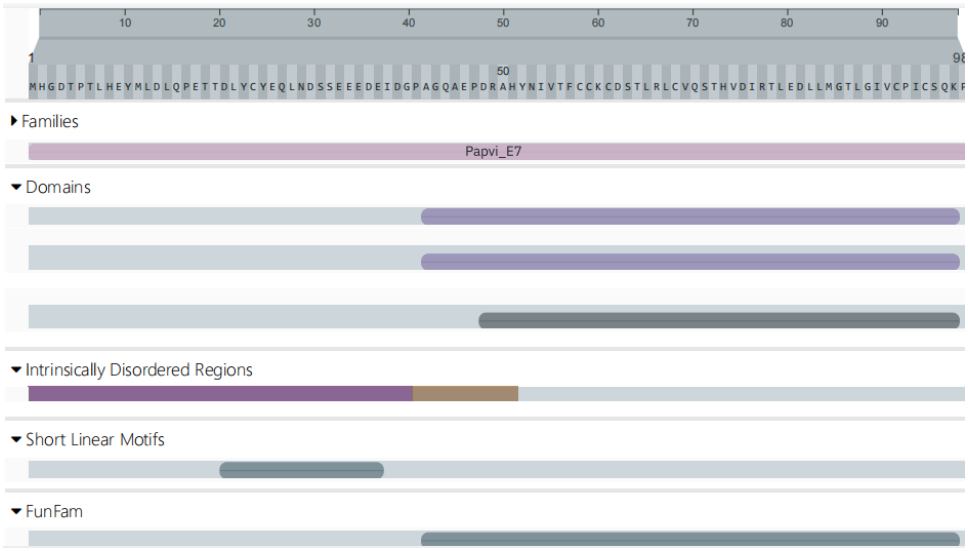

FIGURE 4.3: Functional domain of targeted protein *E7*

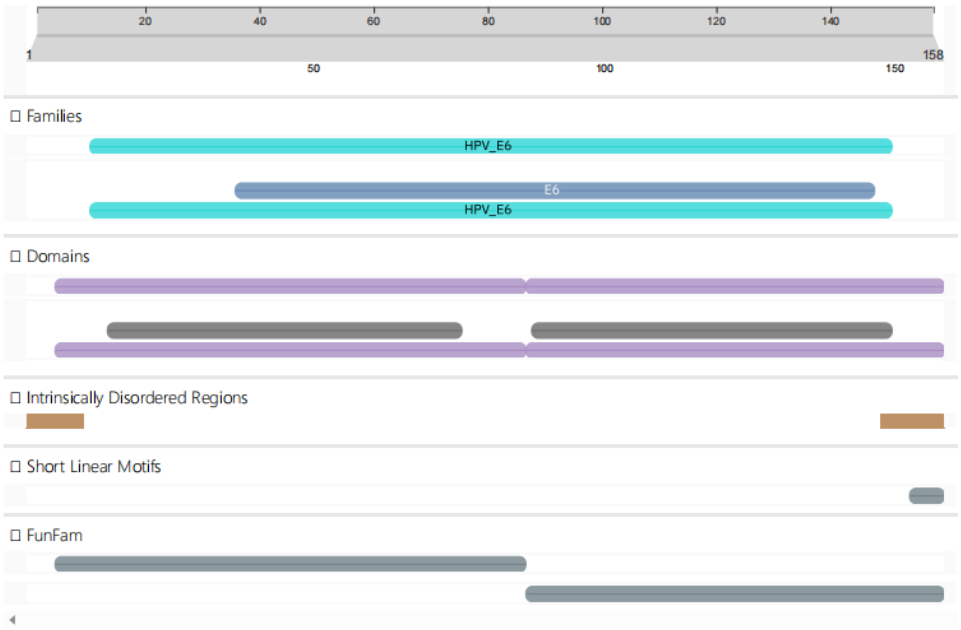

FIGURE 4.4: Functional domain of targeted protein *E6*

4.5 Structure Refinement of Protein for Docking

Before performing molecular docking, the predicted 3D structures of the HPV-16 *E6* and *E7* oncoproteins were refined to ensure accuracy and reliability that are shown in figure 4.5 and 4.6. The structures obtained from the SWISS-MODEL server in .pdb format were first checked visually using PyMOL, where the protein

chains, folding patterns, and surface exposure were carefully observed. Refinement involved the removal of unnecessary components such as water molecules, heteroatoms, and duplicate chains that might interfere with ligand binding.

FIGURE 4.5: Cleaned protein *E6*

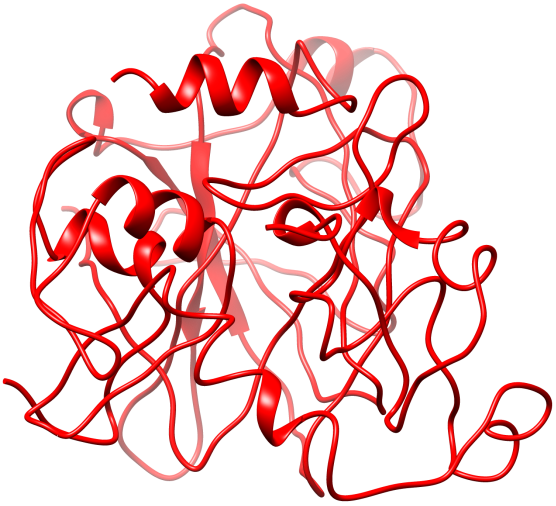

FIGURE 4.6: Cleaned protein *E7*

4.6 Ligand Selection

In this study, the ligands were selected from the medicinal plant *Berberis vulgaris*, which is known for its broad-spectrum pharmacological properties, including antiviral, anticancer, and antimicrobial effects. Based on literature review and availability in the PubChem database, a total of 10–15 bioactive compounds were

shortlisted. These included mainly alkaloids such as berberine, palmatine, jatrorrhizine, columbamine, and berbamine, along with other classes like flavonoids and lignans. The selection criteria were based on their reported activity, presence in *Berberis vulgaris*, and structural compatibility for docking. Each compound was searched on PubChem, and the 3D structure of the molecule was downloaded in .SDF or .PDB format. These ligands were then subjected to further preparation steps, including energy minimization, drug-likeness filtering, and ADMET evaluation.

The selected compounds were expected to bind with the functional domains of *E6* and *E7* oncoproteins and potentially inhibit their oncogenic activity. These ligands were used for molecular docking against the refined protein structures. In Table 4.3 some selected ligands are shown with structural information included Molecular Formula, Molecular Weight and Structure.

TABLE 4.3: Selected ligands with structural information

S. No	**Name**	**Mol Formula**	**Mol Weight**	**Structure**
1.	Berberine	$C_{20}H_{18}NO_4^+$	336.4 g/mol	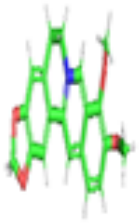
2.	Magnoflorine	$C_{20}H_{24}NO_4^+$	342.4 g/mol	
3.	Jatrorrhizine	$C_{20}H_{20}NO_4^+$	338.4 g/mol	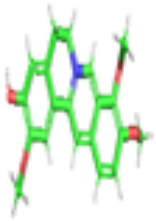

Table 4.3 continued from previous page

S. No	Name	Mol Formula	Mol Weight	Structure
4.	Coptisine	$C_{19}H_{14}NO_4^+$	320.3 g/mol	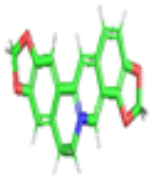
5.	Columbamine	$C_{20}H_{20}NO_4^+$	338.4 g/mol	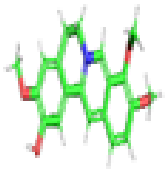
6.	Palmatine	$C_{21}H_{22}NO_4^+$	352.4 g/mol	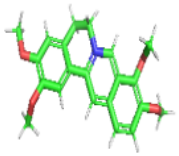
7.	Thalifendine	$C_{19}H_{16}NO_4^+$	322.3 g/mol	
8.	Tetrahydropalmatine	$C_{21}H_{25}NO_4$	355.4 g/mol	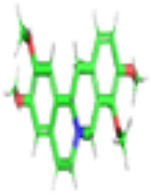
9.	Canadine	$C_{20}H_{21}NO_4$	339.4 g/mol	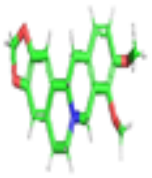
10.	Oxyberberine	$C_{20}H_{17}NO_5$	351.4 g/mol	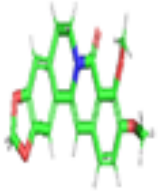
11.	Isocorydine	$C_{20}H_{23}NO_4$	341.4 g/mol	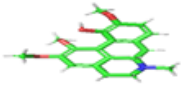

Table 4.3 continued from previous page

S. No	Name	Mol Formula	Mol Weight	Structure
12.	Oxyacanthine	$C_{37}H_{40}N_2O_6$	608.7 g/mol	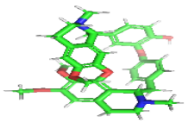
13.	Armepavine	$C_{19}H_{23}NO_3$	313.4 g/mol	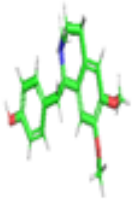
14.	Demethyleneberberine	$C_{21}H_{25}NO_4$	324.3 g/mol	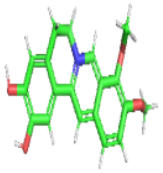
15.	Epiberberine	$C_{20}H_{18}NO_4^+$	336.4 g/mol	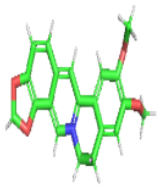

4.7 Virtual Screening and Toxicity Prediction Through Lipinski Rule of Five

To evaluate the drug-likeness and oral bioavailability of the selected ligands from *Berberis vulgaris*, virtual screening was performed using Lipinski's Rule of Five. This rule helps determine whether a compound has suitable properties to be considered a potential drug candidate. The criteria include: molecular weight less than 500 Dalton, no more than 5 hydrogen bond donors, no more than 10 hydrogen bond acceptors, and a logP (partition coefficient) value not greater than 5. Compounds that meet at least three of these criteria are considered to have good oral bioavailability The selected ligands were screened using online tools such as SwissADME and pkCSM, where their SMILES notations were entered to evaluate Lipinski parameters along with additional drug-likeness scores.

Most compounds, especially alkaloids like Magnoflorine, Thalifendine, palmatine, and jatrorrhizine, fulfilled Lipinski's rule and were considered suitable for further molecular docking. The toxicity profile was also evaluated to avoid compounds with high mutagenic or carcinogenic potential. This screening helped prioritize ligands with favorable pharmacokinetic and safety profiles for docking with *E6* and *E7* proteins.Applicability of Lipinski rule on the Ligand are shown in table 4.4.

For compounds to be separated as drug-like and non-drug-like Lipinski rule of five and ADME properties are followed [85]. The Lipinski rule deals with certain parameters like Molecular weight which should be $\leq$ 500, log P $\leq$ 5, H-bond donors $\leq$ 5, H-bond acceptors $\leq$ 10.

These rules are to be followed by orally active compounds. The drug-like is dependent on the mode of administration [87]. A compound is considered a drug when it follows 3 or more rules and if a compound violates two or more rules it is considered poorly absorbed [86].

TABLE 4.4: Applicability of lipinski rule on the ligands

S. No	**Ligand**	**Log P value**	**Mol Weight**	**H-bond Acceptor**	**H-bond Donor**
1	Berberine	2.53	336.4 g/mo	4	0
2	Magnoflorine	0.65	342.4 g/mol	4	0
3	Jatrorrhizine	2.31	338.4 g/mol	4	1
4	Coptisine	2.4	320.3 g/mol	4	0
5	Palmatine	2.64	352.4 g/mol	4	0
6	Thalifendine	2.16	322.3 g/mol	4	1
7	Tetrahydropalmatine	3.08	355.4 g/mol	5	0
8	Canadine	2.97	339.4 g/mol	5	0
9	Oxyberberine	3.04	351.4 g/mo	5	0
10	Isocorydine	2.77	341.4 g/mol	5	1
11	Oxyacanthine	5.13	608.7 g/mol	8	1
12	Armepavine	2.92	313.4 g/mol	4	1
13	Demethyleneberberine	1.89	324.3g/mol	4	2
14	Epiberberine	2.5	336.4 g/mol	4	0
15	Columbamine	2.33	338.4 g/mo	4	1

4.8 Toxicity Prediction of Selected Ligands

To ensure the safety and drug-likeness of the selected ligands from *Berberis vulgaris*, toxicity prediction was performed using the pkCSM online server, which evaluates chemical compounds for potential toxic effects based on their structure. The SMILES notations of each ligand were retrieved from the PubChem database and submitted to pkCSM.

The tool provided a detailed analysis of various toxicity parameters, including AMES toxicity (mutagenicity), maximum tolerated dose in humans, hepatotoxicity, skin sensitization, and oral rat acute toxicity (LD50).

The results showed that most of the selected ligands, particularly Magnoflorine, Thalifendine palmatine, and jatrorrhizine, were non-mutagenic in the AMES test and showed no hepatotoxicity, indicating a favorable safety profile. Compounds with high predicted toxicity or poor safety profiles were excluded from further docking analysis.

This toxicity screening step ensured that only ligands with both strong binding potential and acceptable safety characteristics were carried forward as promising lead candidates against HPV-16 *E6* and *E7* proteins..

4.8.1 Toxicity Value of Berberine and Magnoflorine

The toxicity value of berberine and magnoflorine are given below in table 4.5. It indicated that berberine may be mutagenic while magnoflorine is predicted as non-mutagenic.

Table 4.5: Toxicity value of berberine and magnoflorine

S.No	**Model Name**	**Predicted Value of Berberine**	**Predicted value of Magnoflorine**
1.	AMES Toxicity	Yes	No
2.	Max. tolerated dose (human)	0.438	0.198
3.	hERG I inhibitor	No	No
4.	hERG II inhibitor	No	Yes

Table 4.5 continued from previous page

S.No	Model Name	Predicted Value of Berberine	Predicted value of Magnoflorine
5.	Oral rat acute toxicity	2.482	2.274
6.	Oral rat chronic toxicity	14.732	1.748
7.	Hepatoxicity	No	No
8.	Skin sensitization	No	No
9.	t.pyriformis toxicity	0.285	0.659
10.	Minnow toxicity	8.73	0.954

4.8.2 Toxicity Value of Jatrorrhizine and Coptisine

The toxcity value of jatrorrhizine and coptisine are given below in table 4.6. it indicated that jatrorrhizine is predicted as non-mutagenic while coptisine may be mutagenic.

TABLE 4.6: Toxicity value of jatrorrhizine and coptisine

S.No	Model Name	Predicted value of Jatrorrhizine	Predicted value of Coptisine
1.	AMES Toxicity	No	Yes
2.	Max. tolerated dose (human)	0.175	-0.364
3.	hERG I inhibitor	No	No
4.	hERG II inhibitor	Yes	No
5.	Oral rat acute toxicity	2.445	2.229
6.	Oral rat chronic toxicity	1.356	1.292
7.	Hepatoxicity	Yes	Yes
8.	Skin sensitization	No	No
9.	t.pyriformis toxicity	0.385	0.4
10.	Minnow toxicity	0.177	0.207

4.8.3 Toxicity Value of Palmatine and Thalifendine

The toxicity value of palmatine and thalifendine are given below in table 4.7. It indicated that palmatine may be mutagenic while thalifendine is predicted as non-mutagenic.

TABLE 4.7: Toxicity value of palmatine and thalifendine

S.No	Model Name	Predicted value of Palmatine	Predicted Value of Thalifendine
1.	AMES Toxicity	Yes	No
2.	Max. tolerated dose (human)	0.231	-0.565
3.	hERG I inhibitor	No	No
4.	hERG II inhibitor	Yes	Yes
5.	Oral rat acute toxicity	2.551	2.919
6.	Oral rat chronic toxicity	1.536	1.254
7.	Hepatoxicity	Yes	No
8.	Skin sensitization	No	No
9.	t.pyriformis toxicity	0.388	0.336
10.	Minnow toxicity	-0.313	0.077

4.8.4 Toxicity Value of Tetrahydropalmatine and Canadine

The toxicity value of tetrahydropalmatine and canadine are given below table 4.8. It indicated tetrahydropalmatine and canadine both are mutagenic.

TABLE 4.8: Toxicity value of tetrahydropalmatine and canadine

S.No	Model Name	Predicted Value of Tetrahydropalmatine	Predicted Value of Candine
1.	AMES Toxicity	Yes	Yes
2.	Max. tolerated dose (human)	0.438	0.438
3.	hERG I inhibitor	No	No
4.	hERG II inhibitor	No	No
5.	Oral rat acute toxicity	2.482	2.482
6.	Oral rat chronic toxicity	9.421	9.441
7.	Hepatoxicity	No	No
8.	Skin sensitization	No	No
9.	t.pyriformis toxicity	0.285	0.285
10.	Minnow toxicity	6.846	7.101

4.8.5 Toxicity Value of Oxyberberine and Isocorydine

The toxicity value of oxyberberine and isocorydine are given below in table 4.9. It indicated that oxyberberine may be mutagenic while isocorydine is predicted as non-mutagenic.

TABLE 4.9: Toxicity value of oxyberberine and isocorydine

S.No	**Model Name**	**Predicted value of Oxyberberine**	**Predicted value of Isocorydine**
1.	AMES Toxicity	Yes	No
2.	Max. tolerated dose (human)	0.438	-0.092
3.	hERG I inhibitor	No	No
4.	hERG II inhibitor	No	Yes
5.	Oral rat acute toxicity	2.482	2.66
6.	Oral rat chronic toxicity	11.185	0.733
7.	Hepatoxicity	No	Yes
8.	Skin sensitization	No	No
9.	t.pyriformis toxicity	0.285	0.985
10.	Minnow toxicity	7.17	0.622

4.8.6 Toxicity Value of Oxyacanthine and Armepavine

The toxicity value of oxyacathine and armepavine are given below in table 4.10. It indicated that oxyacanthine may be muatgenic while armepavine is predicted as non mutagenic

TABLE 4.10: Toxicity value of oxyberberine and Armepavine

S.No	**Model Name**	**Predicted value of Oxyberberine**	**Predicted value of Isocorydine**
1.	AMES Toxicity	Yes	No
2.	Max. tolerated dose (human)	0.438	0.06
3.	hERG I inhibitor	No	No
4.	hERG II inhibitor	No	Yes
5.	Oral rat acute toxicity	2.482	2.504
6.	Oral rat chronic toxicity	11.185	1.246
7.	Hepatoxicity	No	Yes

Table 4.10 continued from previous page

S.No	Model Name	Predicted value of Oxyberberine	Predicted value of Armepavine
8.	Skin sensitization	No	No
9.	t.pyriformis toxicity	0.285	1.395
10.	Minnow toxicity	7.17	0.621

4.8.7 Toxcity Value of Glaucine and Epiberberine

The toxicity value of glaucine and epiberberine are given below in table 4.11. It indicated that demethyleneberberine and epiberberine both are mutagenic.

TABLE 4.11: Toxicity value of glaucine and epiberberine

S.No	Model Name	Predicted value of Glaucine	Predicted value of Epibereberine
1.	AMES Toxicity	Yes	Yes
2.	Max. tolerated dose (human)	-0.186	0.438
3.	hERG I inhibitor	No	No
4.	hERG II inhibitor	Yes	No
5.	Oral rat acute toxicity	2.559	2.482
6.	Oral rat chronic toxicity	1.303	12.085
7.	Hepatoxicity	No	No
8.	Skin sensitization	No	No
9.	t.pyriformis toxicity	0.357	0.285
10.	Minnow toxicity	0.568	7.65

4.8.8 Toxicity Value of Columbamine

The toxicity value of columbamine are given below in table 4.12. It indicated that columbamine is predicted as non-mutagenic.

TABLE 4.12: Toxicity value of columbamine

S.No	Model Name	Predicted Value of Columbamine
1.	AMES Toxicity	No
2.	Max. tolerated dose (human)	0.256

Table 4.12 continued from previous page

S.No	Model Name	Predicted Value of Columbamine
3.	hERG I inhibitor	No
4.	hERG II inhibitor	Yes
5.	Oral rat acute toxicity	2.411
6.	Oral rat chronic toxicity	1.42
7.	Hepatoxicity	Yes
8.	Skin sensitization	No
9.	t.pyriformis toxicity	0.398
10.	Minnow toxicity	0.079

4.9 Molecular Docking

Molecular docking was performed to predict the binding interactions between selected bioactive compounds from *Berberis vulgaris* and the HPV16 *E6* and *E7* oncoproteins. The three-dimensional structures of the target proteins were either retrieved from the Protein Data Bank (PDB) or modeled using Swiss-Model based on FASTA sequences from UniProt. Ligands were downloaded in .mol2 format from PubChem and prepared using Chem3D Ultra for energy minimization. Docking was carried out using the CB-Dock2 server, which automatically identifies the top five binding cavities and performs blind docking based on cavity detection. The docking results were evaluated based on binding affinity (Vina score) and cavity volume. Compounds showing more negative binding energy were considered to have stronger and more stable interactions with the target proteins. All docked complexes were visualized using PyMOL and LigPlot to analyze the interaction patterns between the ligand and active site residues..Ligands showing the best binding score between the selected ligands and the proteins *E6* and *E7* are shown in Tables 4.13 - 4.18.

TABLE 4.13: Docking Result of berberine, magnoflorine, jatrorrhizine ,coptisine and palmatine

Compounds	Berberine	Magnoflorine	Jatrorrhizine	Coptisine	Palmatine
Binding Score	-6.7	-7.1	-6.8	-7.3	-1
Cavity size	193	193	193	193	193

Table 4.13 continued from previous page

Compounds	Berberine	Magnoflorine	Jatrorrhizine	Coptisine	Palmatine
HBD	0	0	1	0	0
HBA	4	4	4	4	4
logP	2.53	0.65	2.31	2.4	2.64
Mol Weight	336.4g/mol	342.4g/mol	338.4g/mol	320.3g/mol	352.4g/mol
Bonds	0	2	3	3	4

TABLE 4.14: Docking result of thalifendine, tetrahydropalmatine (THP), canadine, oxyberberine and isocorydine

Compounds	Thalifendine	THP	Canadine	Oxyberberine	Isocorydine
Binding Score	-6.7	-6.7	-6.7	-6.8	-6.9
Cavity size	193	193	193	193	193
HBD	1	0	0	0	1
HBA	4	5	5	5	5
logP	2.16	3.08	2.97	3.04	2.77
Mol Weight	322.3g/mol	355.4	339.4g/mol	351.4g/mol	341.4g/mol
Bonds	1	0	0	0	3

TABLE 4.15: Docking result of oxyacanthine , armepavine, demethyleneberberine (DMB), epiberine and columbamine

Compounds	Oxyacanthine	Armepavine	DMB	Epiberine	Columbamine
Binding Score	-8	-6.8	-6.7	-6.8	-6.6
Cavity size	193	193	193	193	193
HBD	1	1	2	0	1
HBA	8	4	4	4	4
logP	5.13	2.92	1.89	2.5	2.33
Mol Weight	608.7g/mol	313.4g/mol	324.3	336.4	338.4g/mol
Bonds	0	4	2	0	3

4.9.1 Molecular Docking of Selected Ligand with HPV16 *E7* Oncoprotein

Ligands showing the best binding score between the selected ligands and the proteins *E7*.

TABLE 4.16: Docking result of berberine, magnoflorine , jatrorrhizine , coptisine and palmatine

Compounds	**Berberine**	**Magnoflorine**	**Jatrorrhizine**	**Coptisine**	**Palmatine**
Binding Score	-7.1	-6.3	-7.2	-6.5	-6.3
Cavity size	596	119	596	596	596
HBD	0	0	1	0	0
HBA	4	4	4	4	4
logP	2.53	0.65	2.31	2.4	2.64
Mol Weight	336.4g/mol	342.4g/mol	338.4g/mol	320.3g/mol	352.4g/mol
Bonds	0	2	3	3	4

TABLE 4.17: Docking result of thalifendine, tetrahydropalmatine (THP), canadine, oxyberberine and isocorydine:

Compounds	**Thalifendine**	**THP**	**Canadine**	**Oxyberberine**	**Isocorydine**
Binding Score	-7.1	-6.2	-7.1	-6.8	-6.8
Cavity size	596	596	596	193	596
HBD	1	0	0	0	1
HBA	4	5	5	5	5
logP	2.16	3.08	2.97	3.04	2.77
Mol Weight	322.3g/mol	355.4	339.4g/mol	351.4g/mol	341.4g/mol
Bonds	1	0	0	0	3

TABLE 4.18: Docking result of oxyacanthine , armepavine, demethyleneberberine (DMB), epiberberine and columbamine

Compounds	**Oxyacanthine**	**Armepavine**	**DMB**	**Epiberine**	**Columbamin**
Binding Score	-7	-6.2	-7.2	-6.9	-6.4
Cavity size	596	596	596	596	59
HBD	1	1	2	0	1
HBA	8	4	4	4	4
logP	5.13	2.92	1.89	2.5	2.33
Mol Weight	608.7g/mol	313.4g/mol	324.3	336.4g/mol	338.4g/mol
Bonds	0	4	2	0	3

4.10 Interaction of Ligands and Targeted Protein

The result deducted from docking is analyzed through LigPlot and PyMol. The interaction between the Ligands and the receptor protein is predicted through LigPlot+. The graphical system of LigPlot automatically generates the 2D pictures of interactions from its 3d coordinates. The 2D pictures display the hydrogen bond interactions and hydrophobic contacts between the ligand and the main chain or side chain elements of the receptor protein. The 2D diagrams of the interaction of the ligand and the protein. The 2D diagrams of the interaction of the ligands and the protein are shown in figures 4.7 - 4.37.

Figure 4.7 shows the interaction of berberine with receptor protein *E6*. It shows that berberine has formed eight hydrophobic interactions and one hydrogen bond.

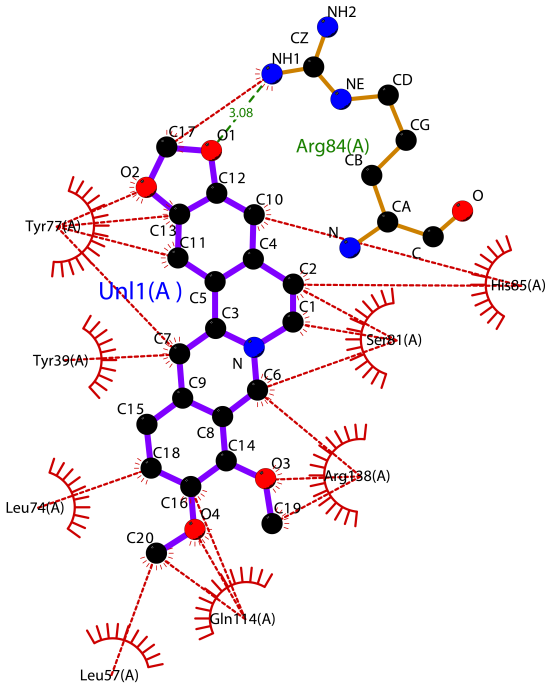

FIGURE 4.7: Interaction of berberine with receptor protein *E6*

Figure 4.8 shows the interaction of magnoflorine with receptor protein *E6*. It shows that magnoflorine has formed eight hydrophobic interactions and four hydrogen bond.

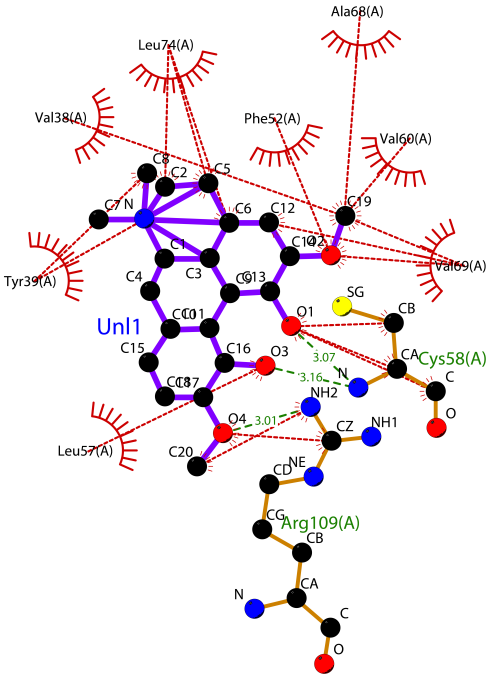

FIGURE 4.8: Interaction of magnoflorine with receptor protein *E6*

Figure 4.9 shows the interaction of jatrorrhizine with receptor protein *E6*. It shows that jatrorrhizine has formed eight hydrophobic interactions and four hydrogen bond.

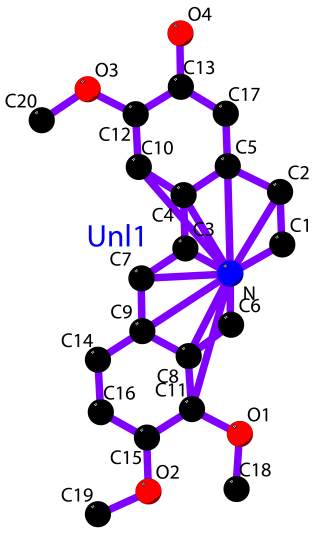

FIGURE 4.9: Interaction of jatrorrhizine with receptor protein *E6*

Figure 4.10 shows the interaction of Coptisine with receptor protein *E6*. It shows that Coptisine has formed eight hydrophobic interactions and four hydrogen bond.

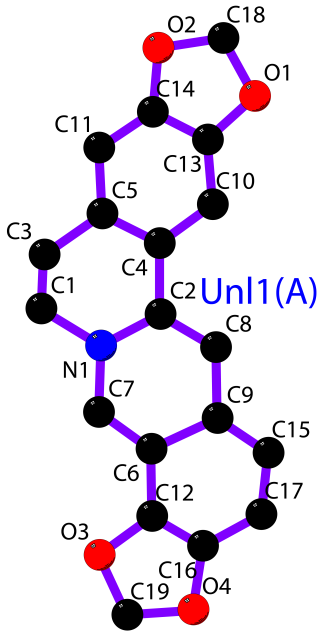

FIGURE 4.10: Interaction of coptisine with receptor protein *E6*

Figure 4.11 shows the interaction of palmatine with receptor protein *E6*. It shows that palmatine has formed five hydrophobic interactions and three hydrogen bond.

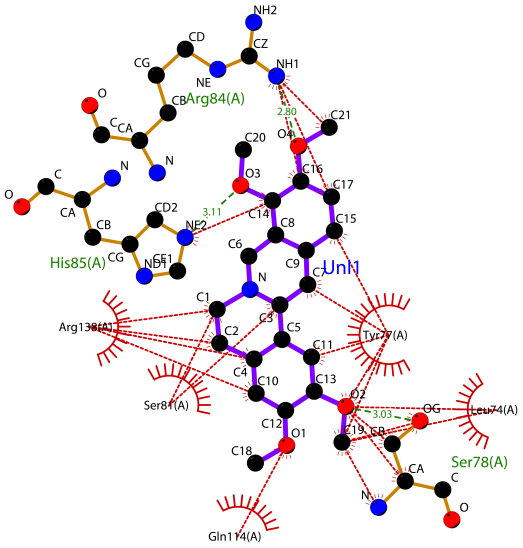

FIGURE 4.11: Interaction of palmatine with receptor protein *E6*

Figure 4.12 shows the interaction of tetrahydropalmatine with receptor protein *E6*. It shows that tetrahydropalmatine has formed twelve hydrophobic interactions.

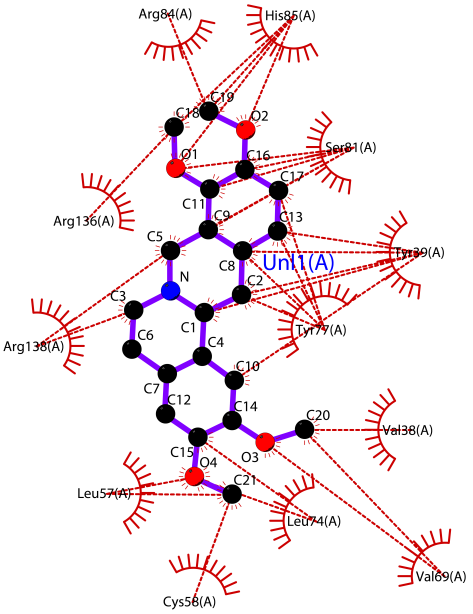

FIGURE 4.12: Interaction of tetrahydropalmatine with receptor protein *E6*

Figure 4.13 shows the interaction of canadine with receptor protein *E6*. It shows that canadine has formed nine hydrophobic interactions.

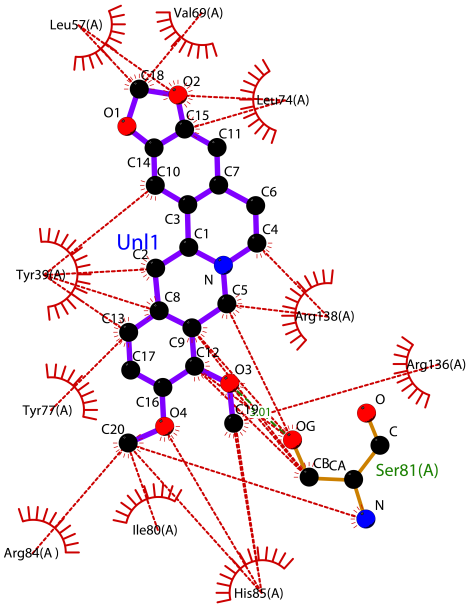

FIGURE 4.13: Interaction of canadine with receptor protein *E6*

Figure 4.14 shows the interaction of oxyberberine with receptor protein *E6*. It shows that oxyberberine has formed nine hydrophobic interactions and two hydrogen bond.

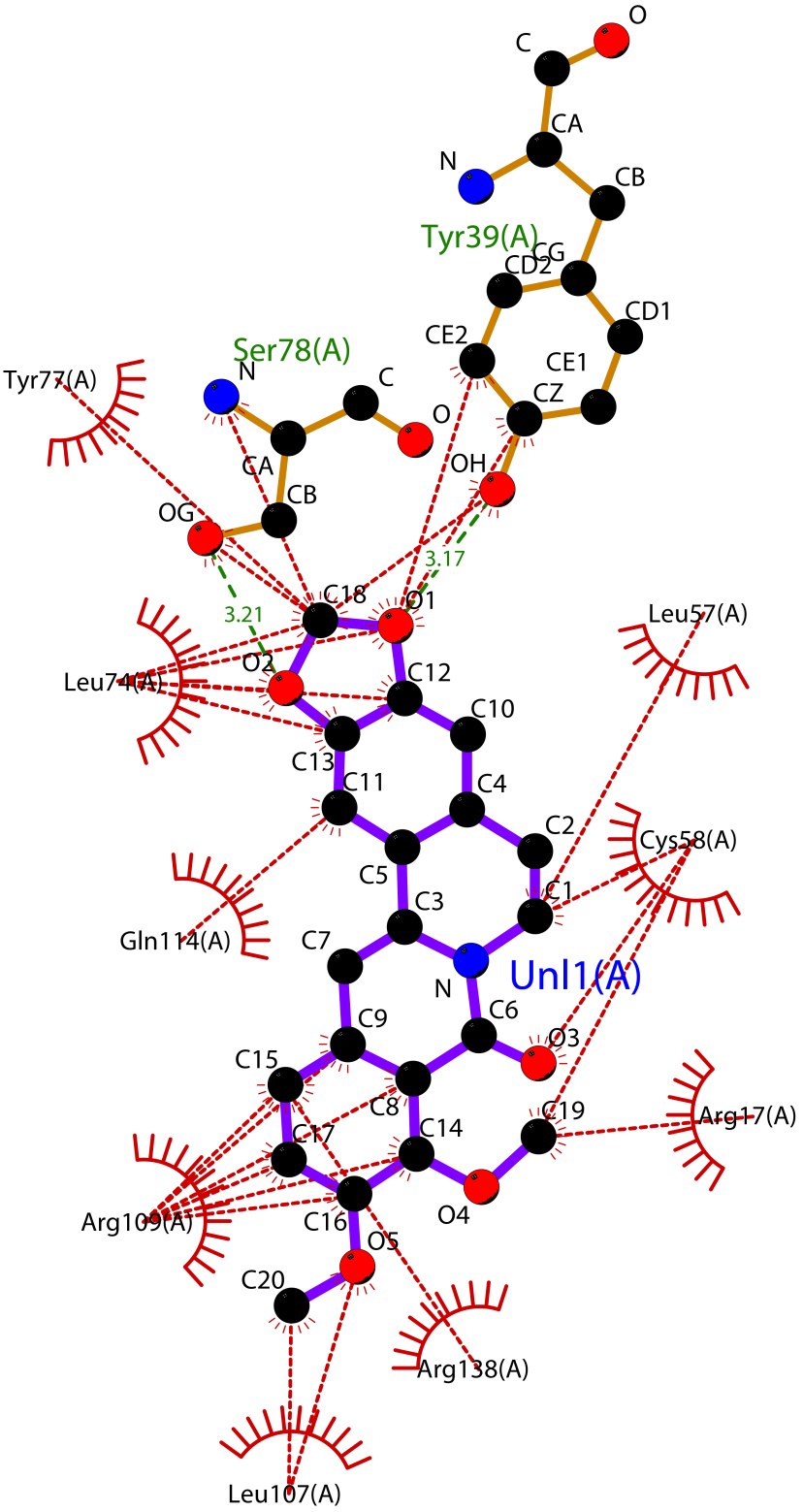

FIGURE 4.14: Interaction of oxyberberine with receptor protein *E6*

Figure 4.15 shows the interaction of Isocorydine with receptor protein *E6*. It shows that Isocorydine has formed eleven hydrophobic interactions.

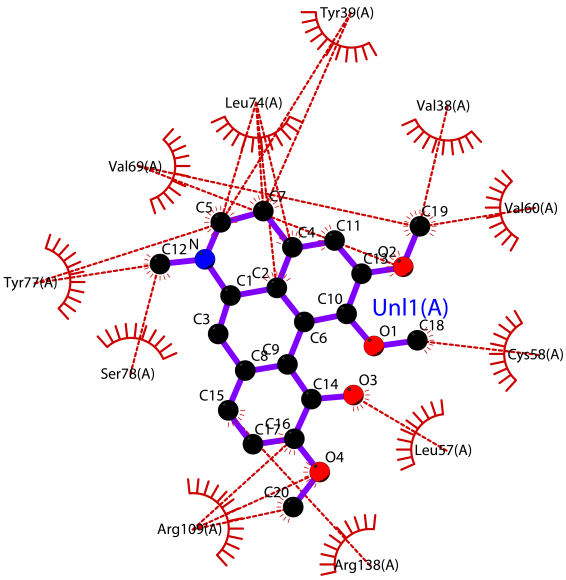

FIGURE 4.15: Interaction of isocorydine with receptor protein *E6*

Figure 4.16 shows the interaction oxyacanthine with receptor protein *E6*. It shows that isocorydine has formed seven hydrophobic interactions and three hydrogen bond.

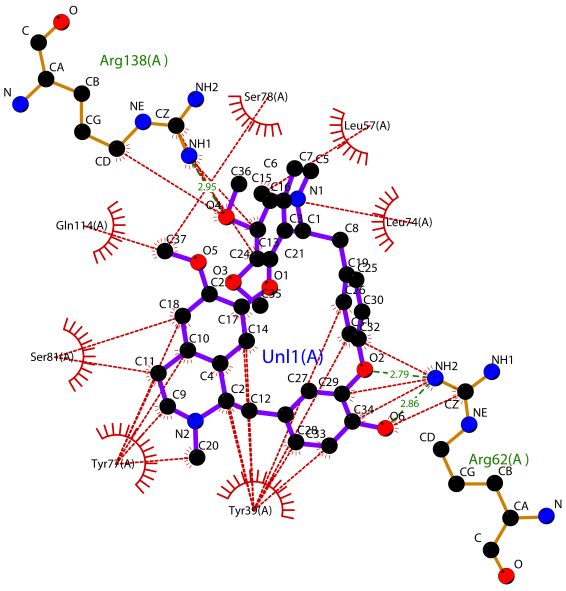

FIGURE 4.16: Interaction of oxyacanthine with receptor protein *E6*

Figure 4.17 shows the interaction armepavine with receptor protein *E6*. It shows that armepavine has formed ten hydrophobic interactions and two hydrogen bond.

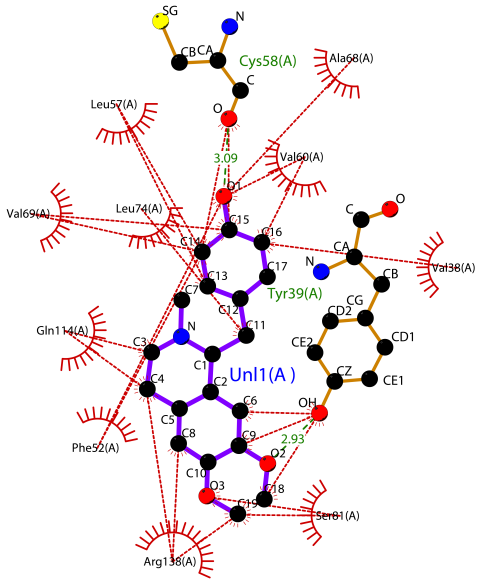

FIGURE 4.17: Interaction of armepavine with receptor protein *E6*

Figure 4.18 shows the interaction Demethyleneberberine with receptor protein *E6*. It shows that Demethyleneberberine has formed eight hydrophobic interactions and three hydrogen bond.

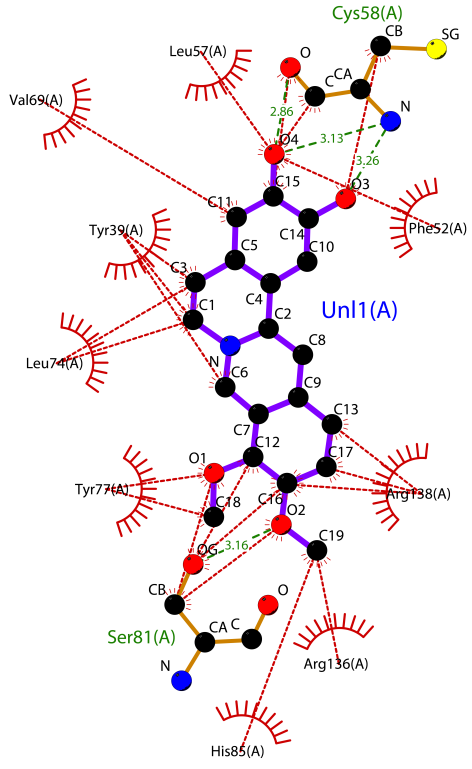

FIGURE 4.18: Interaction of demethyleneberberine with receptor protein *E6*

Figure 4.19 shows the interaction epiberberine with receptor protein *E6*. It shows that epiberberine has formed six hydrophobic interactions and one hydrogen bond.

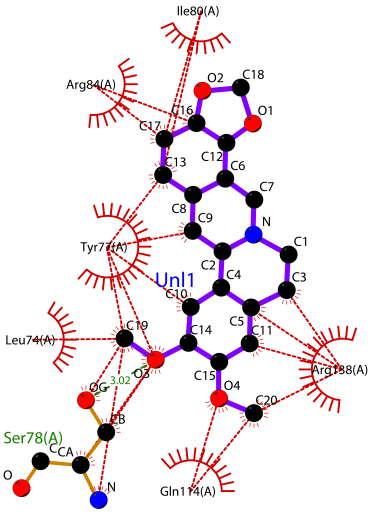

FIGURE 4.19: Interaction of epiberberine with receptor protein *E6*

Figure 4.20 shows the interaction columbamine with receptor protein *E6*. It shows that columbamine has formed four hydrophobic interactions and four hydrogen bond.

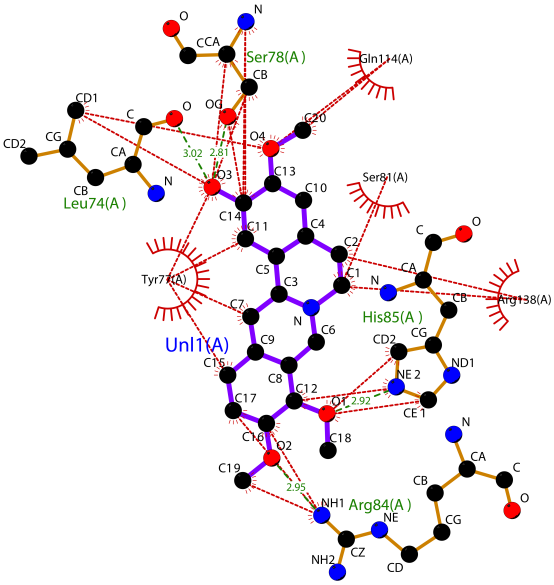

FIGURE 4.20: Interaction of columbamine with receptor protein *E6*

Figure 4.21 shows the interaction thalifendine with receptor protein *E6*. It shows that thalifendine has formed six hydrophobic interactions and one hydrogen bond.

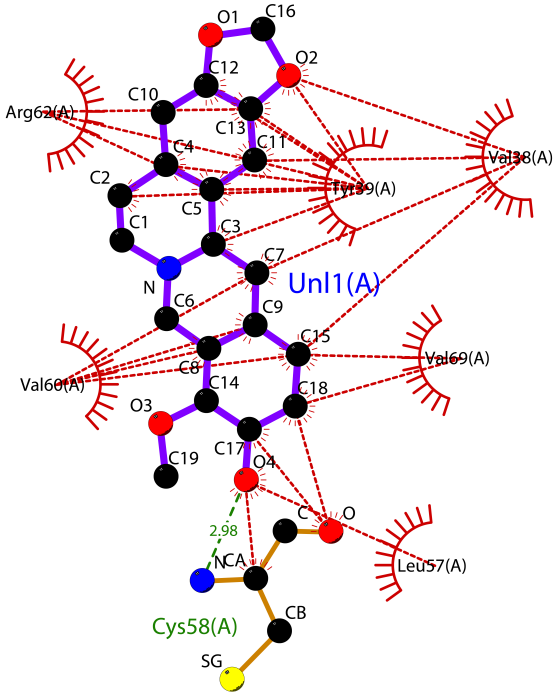

FIGURE 4.21: Interaction of thalifendine with receptor protein *E6*

Figure 4.22 shows the interaction berberine with receptor protein *E7*. It shows that berberine has formed thirteen hydrophobic interactions and two hydrogen bond.

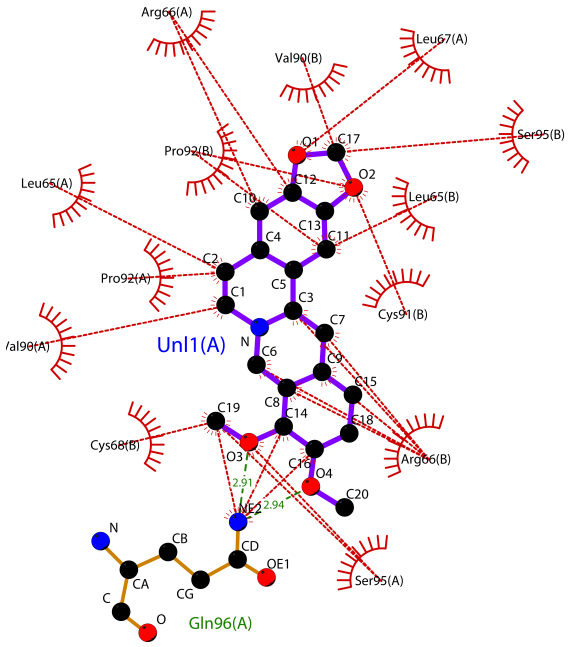

FIGURE 4.22: Interaction of berberine with receptor protein *E7*

Figure 4.23 shows the interaction magnoflorine with receptor protein *E7*. It shows that magnoflorine has formed eight hydrophobic interactions and one hydrogen bond.

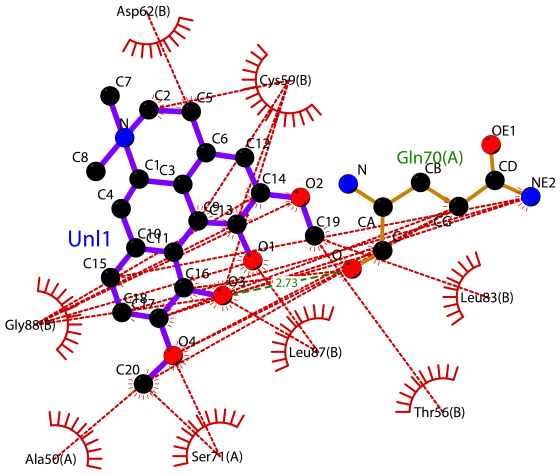

FIGURE 4.23: Interaction of magnoflorine with receptor protein *E7*

Figure 4.24 shows the interaction jatrorrhizine with receptor protein *E7*. It shows that jatrorrhizine has formed eight hydrophobic interactions and three hydrogen bond.

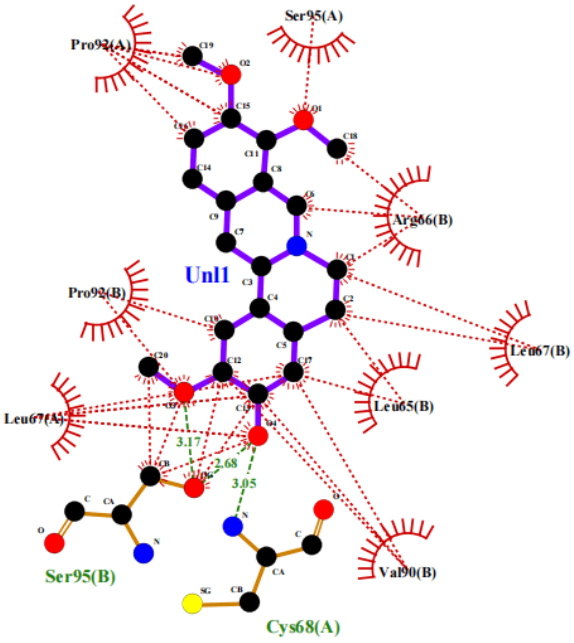

FIGURE 4.24: Interaction of jatrorrhizine with receptor protein *E7*

Figure 4.25 shows the interaction coptisine with receptor protein *E7*. It shows that coptisine has formed eight hydrophobic interactions.

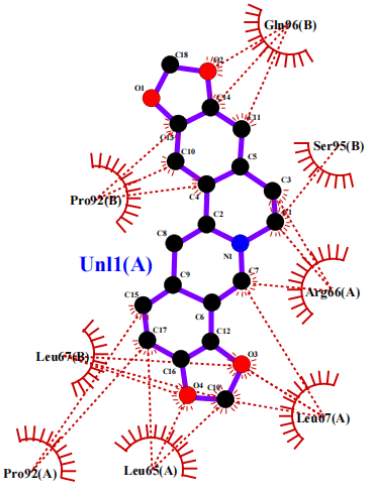

FIGURE 4.25: Interaction of coptisine with receptor protein *E7*

Figure 4.26 shows the interaction Palmatine with receptor protein *E7*. It shows that Palmatine has formed Eight hydrophobic interactions and one hydrogen bond.

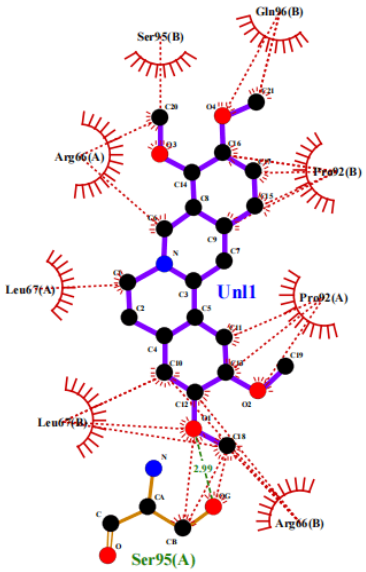

FIGURE 4.26: Interaction of palmatine with receptor protein *E7*

Figure 4.27 shows the interaction thalifendine with receptor protein *E7*. It shows that thalifendine has formed twelve hydrophobic interactions and two hydrogen bond.

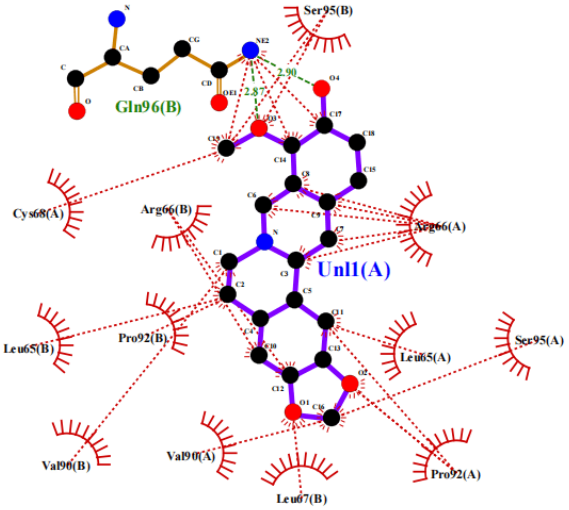

FIGURE 4.27: Interaction of thalifendine with receptor protein *E7*

Figure 4.28 shows the interaction tetrahydropalmatine with receptor protein *E7*. It shows tetrahydropalmatine that has formed twelve hydrophobic interactions and one hydrogen bond.

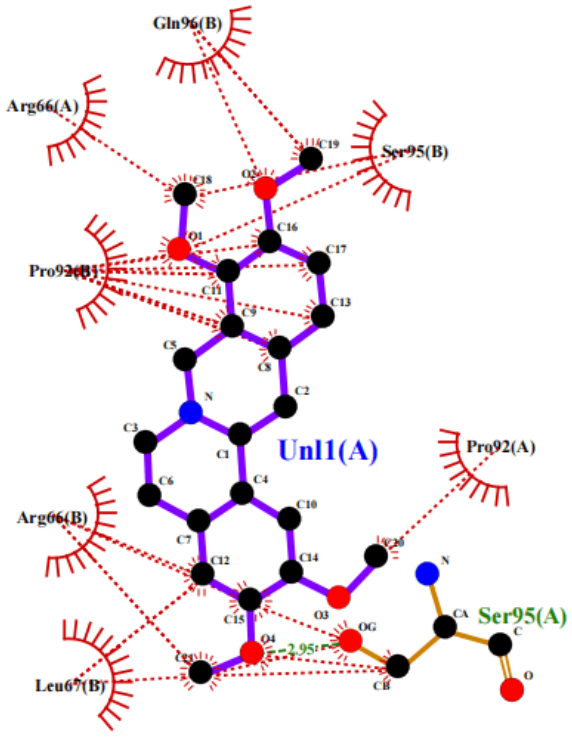

FIGURE 4.28: Interaction of tetrahydropalmatine with receptor protein *E7*

Figure 4.29 shows the interaction canadine with receptor protein *E7*. It shows that has canadine formed twelve hydrophobic interactions and one hydrogen bond.

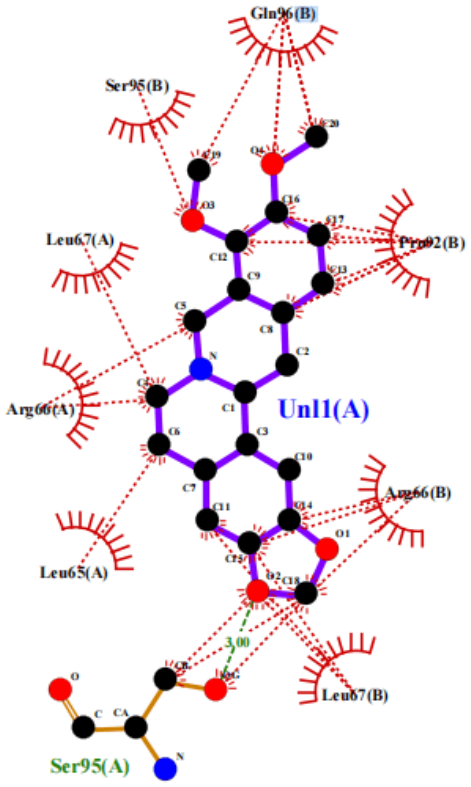

FIGURE 4.29: Interaction of canadine with receptor protein *E7*

Figure 4.30 shows the interaction oxyberberine with receptor protein *E7*. It shows that has oxyberberine formed twelve hydrophobic interactions and three hydrogen bond.

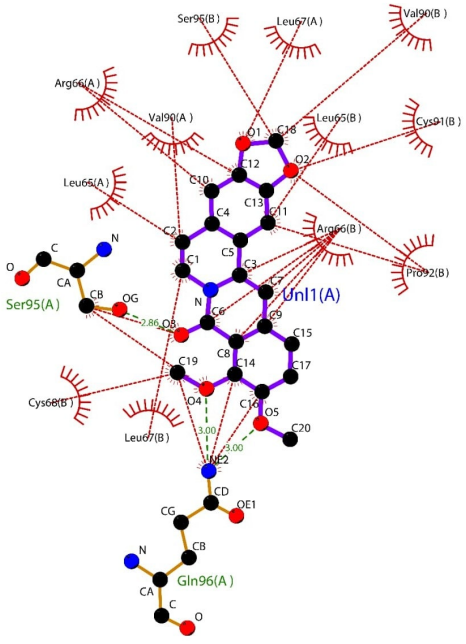

FIGURE 4.30: Interaction of oxyberberine with receptor protein *E7*

Figure 4.31 shows the interaction isocorydine with receptor protein *E7*. It shows that has isocorydine formed eight hydrophobic interactions.

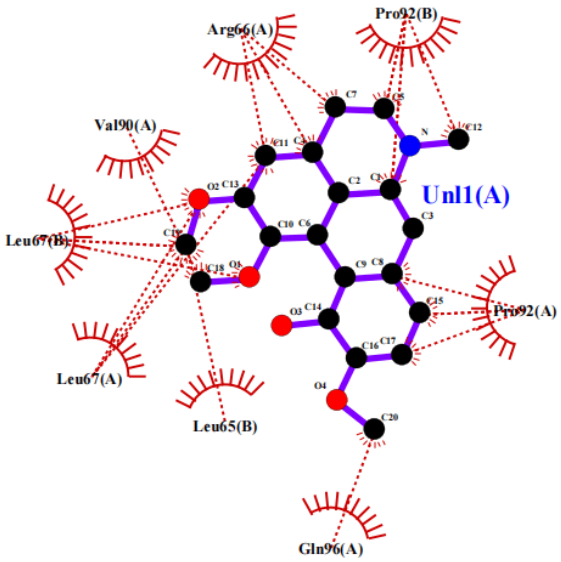

FIGURE 4.31: Interaction of isocorydine with receptor protein *E7*

Figure 4.32 shows the interaction oxyacanthine with receptor protein *E7*. It shows that has oxycanthine formed eight hydrophobic interactions and three hydrogen bond.

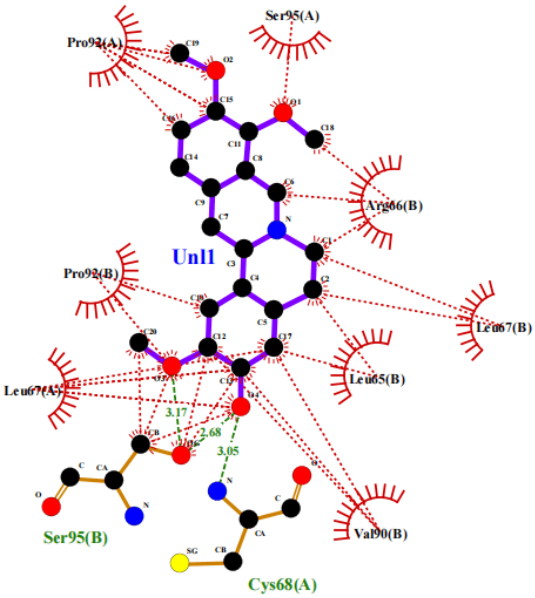

FIGURE 4.32: Interaction of oxycanthine with receptor protein *E7*

Figure 4.33 shows the interaction armepavine with receptor protein *E7*. It shows that has armepavine formed eleven hydrophobic interactions and two hydrogen bond.

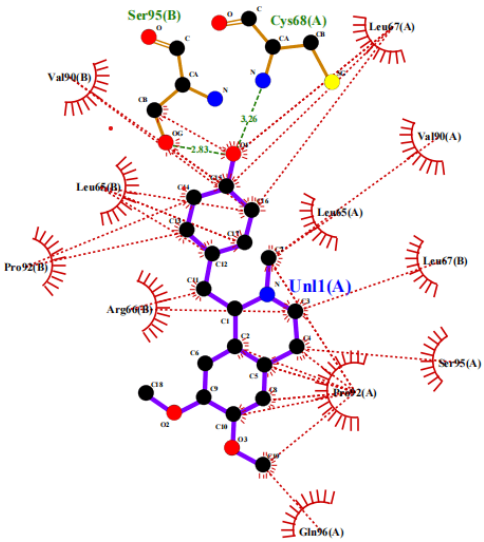

FIGURE 4.33: Interaction of armepavine with receptor protein *E7*

Figure 4.34 shows the interaction demethyleneberberine with receptor protein *E7*. It shows that has demethyleneberberine formed nine hydrophobic interactions and three bond.

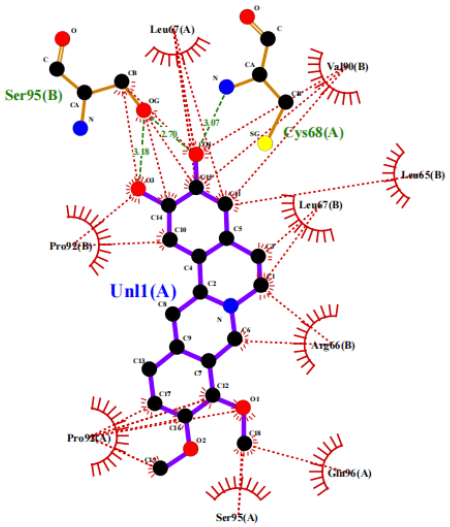

FIGURE 4.34: Interaction of demethyleneberberine with receptor protein *E7*

Figure 4.35 shows the interaction epiberberine with receptor protein *E7*. It shows that has epiberberine formed nine hydrophobic interactions and one hydrogen bond.

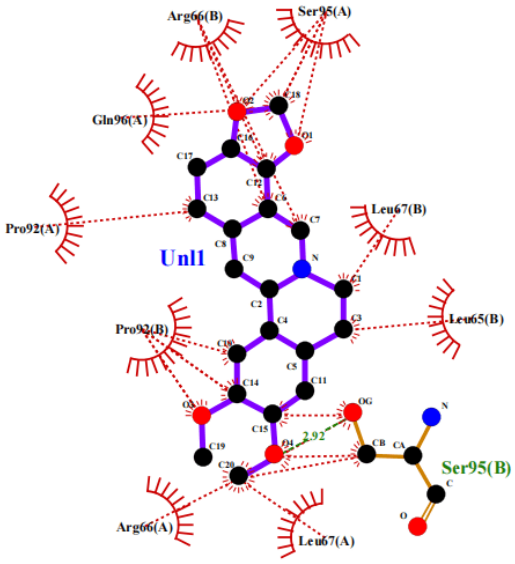

FIGURE 4.35: Interaction of epiberberine with receptor protein *E7*

Figure 4.36 shows the interaction columbamine with receptor protein *E7*. It shows that has columbamine formed seven hydrophobic interactions and four hydrogen bond.

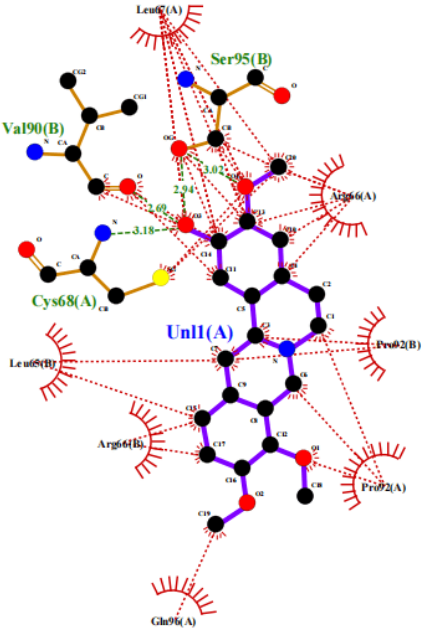

FIGURE 4.36: Interaction of columbamine with receptor protein *E7*

4.11 Active Ligand Showing Hydrogen and Hydrophobic Interactions with Protein *E6*

The table below shows the details of hydrogen and hydrophobic interactions of the selected ligands with the receptor protein. The table provides valuable insights into the interactions between the ligands and the protein. The binding energy values indicate that Coptisine has the strongest interaction with the protein, followed by Magnoflorine, Jatrorrhizine, and Berberine. The number of hydrogen bonds formed between each ligand and the protein also varies, with Berberine forming only one hydrogen bond, while the other three ligands form four hydrogen bonds each.

The hydrogen bonding column reveals that the amino acids involved in hydrogen bonding are Arg14, Cys58, Arg109, and Ser81 for Berberine; Cys58, Arg109, and Ser81 for Magnoflorine; Cys58, Tyr77, and Ser81 for Jatrorrhizine; and Cys58 and Ser81 for Coptisine. The distances between the atoms participating in the hydrogen bonds range from 2.75 to 3.24 Å.The hydrophobic bonding column shows that the amino acids involved in hydrophobic interactions with each ligand are Leu57, Gln14, Arg138, Ser81, His85, Tyr77, Tyr39, and Leu74 for Berberine; Ala61, Val60, Val138, Leu74, Tyr39, Phe52, Val169, and Leu57 for Magnoflorine; Arg136, Tyr77, Arg138, Tyr39, Leu74, Val60, Leu57, and Phe52 for Jatrorrhizine; and Arg136 and Tyr77 for Coptisine.

TABLE 4.19: Active ligand showing hydrogen and hydrophobic interactions with protein E6

S. No.	**Ligand Name**	**Energy**	**No.of HBs**	**Hydrogen Amino acid**	**Bonding Distance**	**Hydrophobic Bonding**
1	Berberine	-6.7	1	Arg84	3.08	Leu57
						Gln114
						Arg138
						Ser81
						His85
						Tyr77
						Tyr39
						Leu74

Table 4.19 continued from previous page

S. No.	Ligand Name	Binding Energy	No.of HBs	Hydrogen Amino acid	Bonding Distance	Hydrophobic Bonding
2	Magnoflorine	-7.1	4	Cys58	2.92	Ala68
				Arg109	3.07	Va160
				Arg109	3.16	Va138
				Arg109	3	Leu74
						Tyr39
						Phe52
						Va169
						Leu57
3	Jatrorrhizine	-6.8	4	Cys58	2.75	Arg136
				Ser81	3.05	Tyr77
				Ser81	3.24	Arg138
				Ser81	3.01	Tyr39
						Leu74
						Val69
						Leu57
						Phe52
4	Coptisine	-7.3	4	Cys58	2.75	Arg136
				Ser81	3.05	Tyr77
				Ser81	3.24	Arg138
				Ser81	3.01	Tyr39
						Leu74
						Val69
						Leu57
						Phe52
5	Columbamine	-6.6	4	Ser78	2.92	Arg138
				Leu78	2.95	Gln114
				His85	2.81	Ser81
				Arg84	3.02	Tyr77
6	Palmatine	-6.6	3	Arg84	2.8	Tyr77
				His85	3.11	Leu74
				Ser78	3.03	Gln114
						Ser81
						Arg138
7	Thalifendine	-6.7	1	Cys58	2.98	Leu57
						Val69

Table 4.19 continued from previous page

S. No.	Ligand Name	Binding Energy	No.of HBs	Hydrogen Amino acid	Bonding Distance	Hydrophobic Bonding
						Va138
						Tyr39
						Arg62
						Va160
8	THP	-6.7	-			Arg84
						His85
						Ser81
						Tyr39
						Tyr77
						Va138
						Va109
						Leu74
						Cys58
						Leu57
						Arg138
						Arg136
9	Canadine	-6.7	-			Arg84
						Tyr77
						Tyr39
						Va169
						Leu57
						Arg138
						His58
						Arg136
10	Oxyberberine	-6.8	2	Tyr39	3.21	Tyr77
				Ser78	3.17	Gln114
						Arg109
						Arg138
						Leu107
						Arg17
						Cys58
						Leu57
						Leu74
11	Isocorydine	-6.9	-			Tyr39
						Va138

Table 4.19 continued from previous page

S. No.	Ligand Name	Binding Energy	No.of HBs	Hydrogen Amino acid	Bonding Distance	Hydrophobic Bonding
						Va160
						Cys58
						Leu57
						Arg138
						Arg109
						Ser78
						Tyr77
						Val69
						Leu74
12	Oxyacanthine	-8	3	Arg138	2.95	Leu74
				Arg62	2.79	Leu57
				Arg62	2.8	Ser78
						Ser81
						Tyr77
						Gln114
						Tyr39
13	Armepavine	-6.8	2	Cys58	3.09	Ala68
				Tyr39	2.93	Val68
						Val38
						Ser81
						Arg138
						Phe52
						Gln114
						Val69
						Leu74
						Leu57
14	BMB	-6.7	4	Ser81	2.86	Phe52
				Cys58	3.13	Arg138
				Cys58	3.26	Arg136
				Cys58	3.16	His85
						Tyr77
						Leu71
						Tyr39
						Val69
						Leu57

Table 4.19 continued from previous page

S. No.	Ligand Name	Binding Energy	No.of HBs	Hydrogen Amino acid	Bonding Distance	Hydrophobic Bonding
15	Epiberberine	-6.8	1	Ser78	3.02	IIe80
						Arg84
						Tyr77
						Leu74
						Arg138
						Gln114

TABLE 4.20: Active ligand showing hydrogen and hydrophobic interactions with protein E7

S. No.	Ligand Name	Binding Energy	No.of HBs	Hydrogen Amino acid	Bonding Distance	Hydrophobic Bonding
1	Berberine	-7.1	2	Gln96	2.91	Cys68
				Gln96	2.94	Arg66
						Ser95
						Cys91
						Leu65
						Leu67
						Val190
						Pro92
2	Magnoflorine	-6.3	1	Gln70	2.73	Asp62
						Cys59
						Thr56
						Leu83
						Ala50
						Leu87
						Ser71
						Gly88
3	Jatrorrhizine	-7.2	3	Ser95	3.17	Ser95
				Cys68	2.68	Arg66
				Cys68	3.05	Leu67
						Leu65
						Val90
						Leu67n
4	Coptisine	-6.5	-			Gln96
						Ser95

Table 4.20 continued from previous page

S. No.	Ligand Name	Binding Energy	No.of HBs	Hydrogen Amino acid	Bonding Distance	Hydrophobic Bonding
						Arg66
						Leu67
						Leu65
						Pro92
5	Columbamine	-6.4	4	Ser95	3.02	Leu67
				Val90	2.94	Arg66
				Cys68	2.69	Pro92
				Cys68	3.18	Gln96
						Leu65
6	Palmatine	-6.3	1	Ser95	2.99	Gln96
						Pro92
						Arg66
						Leu67
7	Thalifendine	-7.1	2	Gln96	2.87	Ser95
				Gln96	2.9	Arg66
						Leu65
						Pro92
						Val92
						Cys66
8	THP	-6.2	1	Ser95	2.95	Gln96
						Ser95
						Pro92
						Leu67
						Arg66
9	Canadine	-7.1	1	Ser95	3	Gln96
						Pro92
						Arg66
						Leu67
						Leu65
						Ser95
10	Oxyberberine	-6.8	3	Gln96	3	Cys68
				Ser95	3	Leu67
				Ser95	2.89	Va190
						Arg66
						Leu65

Table 4.20 continued from previous page

S. No.	Ligand Name	Binding Energy	No.of HBs	Hydrogen Amino acid	Bonding Distance	Hydrophobic Bonding
						Pro92
11	Isocorydine	-6.8	-			Pro92
						Gln96
						Leu65
						Leu67
						Va190
12	Oxyacanthine	-7	3	Ser95	3.17	Ser95
				Cys68	2.68	Arg66
				Cys68	3.05	Leu67
						Leu65
						val90
						Pro92
13	Armepavine	-6.2	2	Ser95	3.26	Leu67
				Cys68	2.83	Val90
						Leu65
						Ser95
						Pro92
						Gln96
14	DMB	-7.2	3	Cys68	3.18	Leu67
				Ser95	2.7	Va190
				Ser95	3.07	Leu65
						Gln96
						Ser95
						Pro92
15	Epiberberine	-6.9	1	Ser95	2.92	Ser95
						Leu67
						Leu65
						Arg66

4.12 ADME Properties of Ligand

Lipinski's five drug law is used as a first step for the assessment of availability either verbal or artificial. pkCSM is the second tool that is used for the assessment of

ADME properties.

4.12.1 Pharmacodynamics

One of the broader terms used in pharmacology is pharmacodynamics which deals with the study of drug effects on the body.

4.12.2 Pharmacokinetics

The other term used in pharmacology is pharmacokinetics which deals with the study of the effect of the body on the drug, that how the body reacts after the drug enters the body. The absorption, distribution, metabolism, and excretion of drugs are also studied.

4.12.3 Absorption

The CaCO2 solubility helps in predicting the absorption of the drugs which are administered orally. Value >0.90 (log Papp in 10-6 cm/s) is considered as high CaCO2 permeability.

The water solubility of the ligands is given as log mol/L. this indicates the compound solubility in water at 25o C. hence the lipid-soluble drugs will be less soluble than the water-soluble drugs.

Intestinal absorption indicates the value or proportion of the compound that will absorb into the intestines. A value less than 30% is considered poorly absorbed.

P-glycoprotein is an ABC transporter that functions to extrude toxins or other xenobiotics from the cells by acting as a biological barrier.

P-glycoprotein inhibition can be a therapeutic target or it can act in contradiction.

Skin permeability is important for developing transdermal drugs. Any compound with a value >-2.5 has a low skin permeability.

Table 4.21 Show the Absorption Properties of Berberine, Magnoflorine, Jatrorrhizine, Coptisine, and Palmatine.Water solubility is negative for all compounds, indicating low solubility in water. CaCO3 solubility varies, with Coptisine having the highest value Intestinal absorption rates are generally high, with berberine showing the highest absorption rate.Skin permeability values are negative, indicating low permeability.Most compounds interact with P-glycoprotein as substrates or inhibitors.

CaCO3 solubility varies, with Coptisine having the highest value Intestinal absorption rates are generally high, with berberine showing the highest absorption rate.Skin permeability values are negative, indicating low permeability.Most compounds interact with P-glycoprotein as substrates or inhibitors.

TABLE 4.21: Absorption Properties of berberine, magnoflorine, jatrorrhizine coptisine and palmatine

Ligands	**Berberine**	**Magnoflorine**	**Jatrorrhizine**	**Coptisine**	**Palmatine**
Water Solubility	-3.973	-3.924	-3.871	-4.014	-2.892
CaCO2 Solubility	1.734	1.575	1.234	2.016	0.472
Intestinal Absorption	97.147	96.107	94.465	98.07	85.783
Skin Permeability	-2.576	-2.758	-2.741	-2.594	-2.735
P-glycoprotein substrate	Yes	Yes	Yes	Yes	No
P-glycoprotein I inhibitor	No	No	No	No	No
P-glycoprotein II inhibitor	Yes	Yes	Yes	Yes	No

Table 4.22 shows the Absorption Properties of thalifendine ,canadine, oxyberberine,tetrahydropalmatine and isocorydine. All compounds have negative water solubility values, indicating low solubility in water. oxyberberine has the lowest water solubility (-4.218), while canadine has the highest (-2.789). The CaCO3 solubility values vary among the compounds. Canadine has the highest CaCO3 solubility (1.626), while tetrahydropalmatine has the lowest (0.679).

TABLE 4.22: Absorption properties of thalifendine, tetrahydropalmatine, canadine, oxyberberine and isocorydine

Ligands	**Thalifendine**	**THP**	**Canadine**	**Oxyberberine**	**Isocorydine**
Water Solubility	-3.397	-3.049	-2.789	-4.218	-3.839
CaCO2 Solubility	1.176	0.679	1.626	1.077	1.178
Intestinal Absorption	96.659	93.104	92.559	100	93.838
Skin Permeability	-2.803	-2.84	-2.93	-2.623	-2.867
P-glycoprotein substrate	Yes	Yes	Yes	No	Yes
P-glycoprotein I inhibitor	No	Yes	No	Yes	Yes
P-glycoprotein II inhibitor	Yes	Yes	Yes	Yes	Yes

The table 4.23 shows the absorption properties of five compounds. Water solubility values range from -3.884 for armepavine to -3.568 for oxyacanthine, indicating varying degrees of solubility in water. Caco3 solubility values range from 0.569 for oxyacanthine to 1.917 for armepavine, suggesting differences in how easily each compound dissolves in a calcium carbonate solution. Intestinal absorption values in humans range from 93.436 for demethyleneberberine to 97.961 for epiberberine, indicating that epiberberine has the highest absorption rate in the human intestine. Skin permeability values range from -2.898 for armepavine to -2.553 for epiberberine, suggesting that epiberberine can pass through the skin more easily than the other compounds.

TABLE 4.23: Absorption properties of oxycanthine, armepavine, demethyleneberberine, epiberberine and columbamine

Ligands	**Oxyacanthine**	**Armepavine**	**DMB**	**Epiberine**	**Columbamine**
Water Solubility	-3.568	-3.884	-3.733	-3.615	-3.836
CaCO2 Solubility	0.569	1.917	0.925	1.87	1.278
Intestinal Absorption	93.476	94.15	93.436	97.961	94.331

Table 4.23 continued from previous page

Ligands	**Oxyacanthine**	**Armepavine**	**DMB**	**Epiberine**	**Columbamine**
Skin Permeability	-2.735	-2.898	-2.738	-2.553	-2.628
P-glycoprotein substrate	Yes	Yes	Yes	Yes	Yes
P-glycoprotein I inh	Yes	Yes	No	No	No
P-glycoprotein II inh	Yes	No	Yes	Yes	Yes

4.12.4 Distribution

The VDss is the theoretical volume which tells about the total dose of the drug which will be needed to be distributed uniformly to give the same concentration as it is in the blood plasma. If the VDss value exceeds 2.81 L/kg, then the drug is more distributed in the tissues than in the plasma.

If the VDss value exceeds 2.81 L/kg, then the drug is more distributed in the tissues than in the plasma. The VDss will be low if the value is below 0.71 L/kg.

Many drugs in the plasma exist in an equilibrium between a bounded and an unbounded state to the serum proteins. As a drug binds more to the serum proteins it will have less efficiency of diffusion to cellular membranes.

The blood-brain barrier protects the brain and reduces the exogenous compounds to enter directly into the brain. If a compound has a value of logBB >0.3 then it will easily cross the BBB barrier hence been effective and if it is logBB<-1 then it is poorly distributed.

Compounds with a value of logPS>-2 penetrate the CNS whereas value logPS<-3 does not penetrate the CNS.

The table 4.24 show the distribution properties of five ligands.berberine, magnoflorine, jatrorrhizine, coptisine, and palmatine. The properties include VDss (human), Fraction unbound (human), BBB Permeability, and CNS Permeability.

TABLE 4.24: Distribution Properties of berberine, magnoflorine, jatrorrhizine, coptisine and palmatine

Ligands	**Berberine**	**Magnoflorine**	**Jatrorrhizine**	**Coptisine**	**Palmatine**
VDss	0.58	1.211	0.539	0.625	0.011
Fraction unbound	0.262	0.105	0.182	0.254	0.381
BBB Permeability	0.198	-0.651	-0.15	-0.062	0.526
CNS Permeability	-1.543	-2.101	-2.142	-1.534	-1.403

The Table 4.25 show the distribution properties of five ligand. Thalifendine , Tetrahydropalmatine, Canadine ,Oxyberberine and Isocorydine. The properties included VDss (human), Fraction unbound (human), BBB Permeability, and CNS Permeability.

The properties included VDss (human), Fraction unbound (human), BBB Permeability, and CNS Permeability.

TABLE 4.25: Distribution properties of thalifendine, tetrahydropalmatine , canadine, oxyberberine and isocorydine

Ligands	**Thalifendine**	**TDP**	**Canadine**	**Oxyberberine**	**Isocorydine**
VDss (human)	0.993	1.024	0.952	0.025	1.029
Fraction unbound	0.239	0.313	0.297	0.168	0.126
BBB Permeability	0.147	0.173	0.13	-0.07	-0.505
CNS Permeability	-2.037	-1.827	-1.832	-2.116	-2.109

The Table 4.26 show the distribution properties of oxyacanthine, armepavine, demethyleneberberine, epiberberine and columbamine may be easily distributed in the body due to their positive value for VDSS and BBB permeability.

Oxyacanthine may not easily distributed in the body due to negative values for VDss and BBB permeability.

TABLE 4.26: Distribution properties of oxyacanthine, armepavine, epiberberine demethyleneberberine and columbamine.

Ligands	**Oxyacanthine**	**Armepavine**	**DMB**	**Epiberberine**	**Columbamine**
VDss (human)	-0.854	1.009	0.58	0.887	0.542
Fraction unbound (human)	0.213	0.145	0.154	0.292	0.288
BBB Permeability	-0.969	0.346	0.066	0.341	-0.181
CNS Permeability	-2.327	-1.347	-2.168	-1.577	-2.142

4.12.5 Metabolism

Cytochrome P450 is an enzyme held responsible for detoxification in the liver. Many drugs get deactivated by this enzyme but certain drugs can be activated. Inhibitors of this enzyme can directly affect the metabolism of drug hence should not be used.

Similarly, CYP2D6 and CYP3A4 are responsible for the metabolism of the drugs. Inhibition to these affects the pharmacokinetics of the drug in use. The Table 4.27 show the Metabolic Properties of Berberine, Magnoflorine, Jatrorrhizine, Coptisine, and Palmatine. The interactions with various CytochromeP 450enzymes, which play a crucial role in drug metabolism.

TABLE 4.27: Metabolic Properties of Berberine,Magnoflorine,Jatrorrhizine Coptisine and Palmatine

Ligands	**Berberine**	**Magnoflorine**	**Jatrorrhizine**	**Coptisine**	**Palmatine**
CYP2D6 sub	No	No	No	No	No
CYP3A4 sub	Yes	Yes	Yes	Yes	No
CYP1A2 inh	Yes	Yes	Yes	Yes	Yes
CYP2C19 inh	No	No	No	No	No
CYP2C9 inh	No	No	No	No	No
CYP2D6 inh	Yes	No	Yes	No	No
CYP3A4 inh	Yes	No	No	Yes	No

The table 4.28 show the Metabolic Properties of Thalifendine , Tetrahydropalmatine , Oxyberberine and Isocorydine. The interaction with various CytochromeP 450enzymes, which play a crucial role in drug metabolism.

TABLE 4.28: Metabolic Properties of Thalifendine ,Tetrahydropalmatine ,Canadine, Oxyberberine and Isocorydine:

Ligands	**Thalifendine**	**TDP**	**Canadine**	**Oxyberberine**	**Isocorydine**
CYP2D6 sub	No	No	No	No	No
CYP3A4 sub	Yes	Yes	Yes	Yes	Yes
CYP1A2 inh	Yes	Yes	Yes	Yes	Yes
CYP2C19 inh	No	No	No	Yes	No
CYP2C9 inh	No	No	No	No	Yes
CYP2D6 inh	Yes	Yes	Yes	No	No
CYP3A4 inh	No	No	No	Yes	No

The table 4.29 show the metabolic properties of five compounds: Oxyacanthine, Armepavine, De methylene berberine, Epiberberine, and Columbamine. It details their interactions with various cytochrome P450 enzymes, crucial for drug metabolism.

Oxyacanthine and Armepavine are substrates for CYP3A4, while Demethyleneberberine, Epiberberine, and Columbamine are not.Armepavine is a substrate for CYP1A2 and CYP2C19, and Oxyacanthine is a substrate for CYP2D6. None of the compounds are substrates for CYP2C9 or CYP1A1. All five compounds inhibit CYP3A4.

TABLE 4.29: Metabolic Properties of Oxyacanthine, Armepavine, Demethyleneberberine,Epiberberine and Columbamine

Ligands	**Oxyacanthine**	**Armepavine**	**DMB**	**Epiberberine**	**Columbamine**
CYP2D6 sub	Yes	Yes	No	No	No
CYP3A4 sub	Yes	Yes	Yes	Yes	Yes
CYP1A2 inh	No	Yes	Yes	Yes	Yes
CYP2C19 inh	Yes	No	No	No	No
CYP2C9 inh	No	No	No	No	No
CYP2D6 inh	No	Yes	Yes	Yes	Yes
CYP3A4 inh	No	No	No	No	No

4.13 Excretion

The Renal OCT2 substrate acts as a transporter that helps in clearing the drugs and other compounds. Total clearance indicates hepatic clearance which means the drug is metabolized and renal clearance indicates the drug is excreted. The excretion values of the ligands are given below.

The table 4.30 shows the excretion properties of five compounds: Berberine, Magnoflorine, Jatrorrhizine, Coptisine, and Palmatine. Berberine has a total clearance value of 1.27, Magnoflorine has a value of 0.833, Jatrorrhizine has a value of 1.222, Coptisine has a value of 1.28, and Palmatine has a value of -0.266.

TABLE 4.30: Excretion Properties of berberine, magnoflorine, jatrorrhizine coptisine and palmatine

Ligands	**Berberine**	**Magnoflorine**	**Jatrorrhizine**	**Coptisine**	**Palmatine**
Total Clearance	1.27	1.083	1.222	1.28	-0.266
Renal OCT2 Substrate	No	No	No	Yes	No

The Table 4.31 show the excretion properties of five additional compounds: Thalifendine, tetrahydropalmatine, Canadine, Oxyberberine, and Isocorydine.the total clearance values for each compound, which are 1.244 for Thalifendine, 1.123 for Tetrahydropalmatine, 1.144 for Canadine, 0.121 for Oxyberberine, and 0.398 for Isocorydine.

TABLE 4.31: Excretion Properties of thalifendine ,tetrahydropalmatine ,canadine, oxyberberine and isocorydine

Ligands	**Thalifendine**	**TDP**	**Canadine**	**Oxyberberine**	**Isocorydine**
Total Clearance	1.244	1.123	1.144	0.121	0.998
Renal OCT2 Substrate	No	No	No	Yes	No

The Table 4.32 show the excretion properties of Oxyacanthine, Armepavine, De methylene berberine, Epiberberine, and Columbamine. The total clearance values:

0.719 for Oxyacanthine, 1.926 for Armepavine, 1.204 for Demethyleneberberine, 1.178 for Epiberberine, and 1.224 for Columbamine.

TABLE 4.32: Excretion properties of oxyacanthine, armepavine, demethyleneberberine, epiberberine and columbamine

Ligands	**Oxyacanthine**	**Armepavine**	**DMB**	**Epiberberine**	**Columbamine**
Total Clearance	0.719	1.026	1.204	1.278	1.224
Renal OCT2 Substrate	No	Yes	No	Yes	No

4.14 Lead Compound Identification

Based on comprehensive in silico screening, Magnoflorine and Thalifendine were identified as the most promising lead compounds targeting the *E6* and *E7* oncoproteins of HPV16.

Based on comprehensive in silico screening, Magnoflorine and Thalifendine were identified as the most promising lead compounds targeting the *E6* and *E7* oncoproteins of HPV16. Magnoflorine demonstrated a strong binding affinity with *E6* (-7.1 kcal/mol) and moderate affinity with *E7* (-6.4 kcal/mol), while Thalifendine showed the reverse trend, exhibiting a good docking score with *E6* (-6.7 kcal/mol) and a stronger interaction with *E7* (-7.1 kcal/mol).

Both compounds complied with Lipinski's Rule of Five, indicating favorable oral bioavailability. Toxicity predictions revealed that neither compound showed any AMES toxicity, hepatotoxicity, nor skin sensitization, confirming their potential safety. These findings suggest that Magnoflorine and Thalifendine possess the desired pharmacokinetic and pharmacodynamic properties, making them suitable lead candidates for further experimental validation and potential antiviral drug development against HPV.

4.15 Drug Identification against Human Papillomavirus Types 16

In this study, Imiquimod was selected as the reference standard drug for comparison. Imiquimod is a clinically approved topical agent used to treat external genital and perianal warts caused by Human Papillomavirus, including HPV16. Although it does not directly inhibit the viral oncoproteins, it acts by stimulating the innate immune response, primarily through the induction of cytokines such as interferon-α, tumor necrosis factor-α, and interleukins.

Due to its established clinical use, safety profile, and therapeutic relevance, Imiquimod was chosen as the benchmark molecule for evaluating the docking and drug-likeness performance of selected bioactive compounds in this study [86, 87].

4.15.1 Imiquimod

Imiquimod is a synthetic imidazoquinoline compound that functions as an immune response modifier. It is widely used as a topical treatment for external genital and perianal warts caused by Human Papillomavirus (HPV), including high-risk types such as HPV16. Imiquimod does not directly target viral proteins like *E6* or *E7*, but rather exerts its therapeutic effect by stimulating the innate immune system.

It activates toll-like receptor 7 (TLR7) on immune cells, leading to the production of pro-inflammatory cytokines such as interferon-α (IFN-α), tumor necrosis factor-alpha (TNF-α), and interleukins, which enhance the clearance of virus-infected cells. Clinically, a 5% topical cream formulation of imiquimod is approved for the treatment of genital warts, actinic keratosis, and superficial basal cell carcinoma. Its inclusion as a reference standard in in silico studies is valuable for evaluating the relative performance of novel compounds in terms of binding affinity, drug-likeness, and safety [86, 87].

4.15.2 Toxicity Prediction of Reference Drug

The Table 4.33 show the predicting toxicity ,including AMES toxicity ,maximum tolerated does in dose in humans, hERG I inhibitor, hERG II inhibitor, oral rat acute toxicity, oral rat chronic toxicity, hepatotoxicity, skin sensitization, T.pyriformis toxicity, and minnow toxicity. The toxicity prediction of imiquimod using various models. The results indicate that imiquimod has varying levels of toxicity depending on the model used, with some models predicting high toxicity and others predicting low toxicity.

The results indicate that imiquimod has varying levels of toxicity depending on the model used, with some models predicting high toxicity and others predicting low toxicity.

TABLE 4.33: Toxicity Prediction of Imiquimod

S.No	Model Name	Predicted Value
1	AMES Toxicity	Yes
2	Max. tolerated dose (human)	0.675
3	hERG I inhibitor	No
4	hERG II inhibitor	No
5	Oral rat acute toxicity	2.665
6	Oral rat chronic toxicity	0.817
7	Hepatoxicity	Yes
8	Skin sensitization	No
9	t.pyriformis toxicity	0.285
10	Minnow toxicity	0.174

4.15.3 Absorption Properties of Reference Drug

The table 4.34 various absorption properties of Imiquimod, including water solubility (-2.796), CaCO3 solubility (1.238), intestinal absorption (92.046%), and skin permeability (-2.736).

Additionally, it indicates whether Imiquimod is a substrate or inhibitor of P-glycoprotein I and II.

TABLE 4.34: Absorption Properties of Imiquimod

S. No.	Reference drug	Imiquimod
1	Water Solubility	-2.796
2	CaCO2 Solubility	1.238
3	Intestinal Absorption (human)	92.046
4	Skin Permeability	-2.736
5	P-glycoprotein substrate	Yes
6	P-glycoprotein I inhibitor	No
7	P-glycoprotein II inhibitor	No

4.15.4 Distribution Properties of Reference Drug

The Table 4.35 show the distribution properties of Imiquimod, including its volume of distribution (VDss) of 0.736, fraction unbound of 0.141, BBB permeability of 0.212, and CNS permeability of -2.051.

TABLE 4.35: Distribution Properties of Imiquimod

S. No.	Reference Drug	Imiquimod
1	VDss (human)	0.736
2	Fraction unbound (human)	0.141
3	BBB Permeability	0.212
4	CNS Permeability	-2.051

4.15.5 Metabolic Properties of Reference Drug

The Table 4.36 show the metabolic properties of Imiquimod ,included CYP2D6 substrate, CYPEA4substrate ,CYPLA2 inhibitor, CYP2CL9 inhibitor, CYPZC9 inhibitor, CYP2D6 inhibitor, CYP3A4 inhibitor.

TABLE 4.36: Metabolic Properties of Imiquimod

S. No	Reference Drug	Imiquimod
1	CYP2D6 substrate	No
2	CYP3A4 substrate	No
3	CYP1A2 inhibitor	Yes

Table 4.36 continued from previous page

S. No	Reference Drug	Imiquimod
4	CYP2C19 inhibitor	Yes
5	CYP2C9 inhibitor	No
6	CYP2D6 inhibitor	No
7	CYP3A4 inhibitor	No

4.15.6 Excretion Properties of Reference Drug

The Table 4.37 show the excretion Properties of Imiquimod. The total clearance of Imiquimod is 0.79, indicating the rate at which it is removed from the body. Imiquimod is a substrate for the OCT2 transporter, which is involved in its renal excretion.

TABLE 4.37: Excretion properties of Imiquimod

S. No.	Reference Drug	Imiquimod
1	Total Clearance	0.79
2	Renal OCT2 Substrate	Yes

4.15.7 Imiquimod Mechanism of Action

Imiquimod functions primarily as an immune response modifier by activating the innate immune system. Its main mechanism involves binding to Toll-like receptor 7 (TLR7), which is expressed on dendritic cells, macrophages, and monocytes. Upon activation, TLR7 triggers intracellular signaling cascades that lead to the production of pro-inflammatory cytokines, including interferon-alpha (IFN-α), interleukin-6 (IL-6), interleukin-12 (IL-12), and tumor necrosis factor-alpha (TNF-α). These cytokines enhance the antiviral immune response, promote the activation of natural killer cells and cytotoxic T cells, and stimulate antigen presentation. As a result, virus-infected cells, such as those harboring HPV16, are identified and eliminated by the immune system. Imiquimod is typically used in topical formulations (e.g., 5% cream) for treating external genital warts, precancerous skin lesions, and superficial basal cell carcinoma [91].

4.15.8 Imiquimod Effects on Body

Imiquimod exerts its therapeutic effect by stimulating the natural defense system particularly through initiation of Toll-like receptor 7 (TLR7)defensive cells such as dendritic cells and macrophages. This leads to increased production of pro-inflammatory cytokines, including interferon-alpha (IFN-α), interleukin-6 (IL-6), interleukin-12 (IL-12), and tumor necrosis factor-alpha (TNF-α), which together enhance antiviral activity, tumor suppression, and immune cell recruitment. These immune-stimulating effects allow the body to recognize and destroy virus-infected or abnormal cells, such as those caused by HPV infection. Topically, Imiquimod is used to check the management of genital warts, actinic keratosis, and early-stage skin cancer.However, because of its strong immune-activating properties, it may also cause localized side effects such as redness, swelling, itching, or burning at the site of application. In some cases, systemic flu-like symptoms (e.g., fatigue, fever, headache) may also occur, especially if applied over large areas or for prolonged periods.

4.15.9 Imiquimod Docking with Protein *E6*

The Table 4.38 show the interaction between Imiquimod and Protein *E6*.

TABLE 4.38: Docking result of Imiquimod

Compound	**Score**	**Cavity**	**HBD**	**HBA**	**logP**	**Mol Weight**	**Bonds**
Imiquiomod	-6.5	193	1	4	2.8227	240.31	2

4.15.10 Imiquimod Docking with Protein *E7*

The Table 4.39 show the interaction between Imiquimod and Protein *E7*.

TABLE 4.39: Docking result of Imiquimod

Compound	**Score**	**Cavity**	**HBD**	**HBA**	**logP**	**Mol Weight**	**Bonds**
Imiquiomod	-6	596	1	4	2.8227	240.31	2

4.15.11 Imiquimod Comparison with Lead Compound

To evaluate the antiviral potential of plant-derived ligands, the clinically approved drug Imiquimod was employed as a comparative standard. Molecular docking analysis revealed that Imiquimod exhibited moderate binding affinity toward the *E6* and *E7* oncoproteins of HPV16. In comparison, the bioactive compounds Magnoflorine and Thalifendine, isolated from *Berberis vulgaris*, showed competitive or superior docking scores. Thalifendine displayed a stronger interaction with *E7* (-7.1 kcal/mol) than Imiquimod, while Magnoflorine exhibited stronger binding with *E6* (-7.1 kcal/mol). Both lead compounds complied with Lipinski's Rule of Five, showed no toxicity or hepatotoxicity, and formed favorable hydrogen and hydrophobic interactions at the active site.

These findings suggest that natural compounds such as Magnoflorine and Thalifendine may serve as potential alternatives or complementary agents to existing therapies like Imiquimod for HPV16-related infections.

These findings suggest that natural compounds such as Magnoflorine and Thalifendine may serve as potential alternatives or complementary agents to existing therapies like Imiquimod for HPV16-related infections.

Table 4.40: Lipinski Rule Comparison

Name	**Log P-value**	**Mol Weight**	**H-bond acceptor**	**H-bond donor**
Imiquiomod	2.8227	240.31	4	1
Magnoflorine	0.65	342.4	4	0
Thalifendine	2.16	322.3	4	1

4.15.12 ADMET Properties Comparison

The ADMET properties of all drugs and lead compounds are compared to evaluate their absorption, distribution, metabolism, excretion, and toxicity, with the aim of identifying the most suitable drug candidate.

4.15.13 Toxicity Comparison

The safety profiles of Imiquimod, Magnoflorine, and Thalifendine were evaluated using in silico toxicity prediction tools to assess their drug-likeness and potential adverse effects.

Imiquimod, although clinically approved, exhibited a moderate immune-activating profile, and in some cases has been associated with localized skin irritation and flu-like systemic effects.

In contrast, the selected lead compounds from *Berberis vulgaris*, Magnoflorine and Thalifendine, showed no predicted AMES toxicity, hepatotoxicity, or skin sensitization in ADMET analysis, indicating a favorable toxicity profile. This comparison highlights that these natural compounds show promise as safer alternatives or supportive agents to existing antiviral drugs in the treatment of HPV16-associated infections.

Table 4.41: Toxicity Properties Comparison

S.No	Model Name	Imiquiomod	Magnoflorine	Thalifendine
1	AMES Toxicity	Yes	No	No
2	Max. tolerated dose (human)	0.675	-0.565	0.198
3	hERG I inhibitor	No	No	No
4	hERG II inhibitor	No	Yes	Yes
5	Oral rat acute toxicity	2.665	2.919	2.274
6	Oral rat chronic toxicity	0.817	1.254	1.748
7	Hepatoxicity	Yes	No	No
8	Skin sensitization	No	No	No
9	t.pyriformis toxicity	0.285	0.336	0.659
10	Minnow toxicity	0.174	0.077	0.954

4.15.14 Absorption Properties Comparison

The comparative evaluation of the assimilation properties of Imiquimod, Magnoflorine, and Thalifendine revealed that all three compounds possess favorable

characteristics for efficient drug absorption. Imiquimod, used clinically as a topical agent, showed high gastrointestinal (GI) absorption, consistent with its effective skin permeability. Similarly, the plant-derived compounds Magnoflorine and Thalifendine also exhibited high predicted GI absorption, indicating their potential for oral bioavailability. Importantly, none of the compounds were predicted to be P-glycoprotein (P-gp) substrates, reducing the likelihood of efflux from intestinal epithelial cells and enhancing their intracellular retention. This uniformity in absorption behavior supports the drug-likeness of the natural compounds in comparison to the standard drug, Imiquimod.

TABLE 4.42: Absorption Properties Comparison

Mosel Name	**Imiquiomod**	**Magnoflorine**	**Thalifendine**
Water Solubility	-2.796	-3.924	-3.397
CaCO2 Solubility	1.238	1.575	1.176
Intestinal Absorption (human)	92.046	96.107	96.659
Skin Permeability	-2.736	-2.758	-2.803
P-glycoprotein substrate	Yes	Yes	Yes
P-glycoprotein I inhibitor	No	No	No
P-glycoprotein II inhibitor	No	Yes	Yes

4.15.15 Metabolic Properties Comparison

The metabolism of drug candidates plays a critical role in determining their efficacy and safety. In silico metabolism predictions were carried out to assess the interaction of Imiquimod, Magnoflorine, and Thalifendine with major cytochrome P450 (CYP) enzymes. Imiquimod was predicted to be a non-inhibitor of major CYP isoforms, suggesting a lower risk of metabolic drug–drug interactions. Similarly, both Magnoflorine and Thalifendine were also predicted not to inhibit key CYP450 enzymes such as CYP3A4, CYP2D6, CYP1A2, CYP2C19, and CYP2C9, that lead to the biotransformation of a extensive variety of pharmaceuticals. This non-inhibitory profile indicates a favorable metabolic stability for the natural compounds, comparable to that of the standard drug Imiquimod. Their ability to avoid

CYP450 inhibition enhances the potential for safe combination therapy without interfering with the metabolism of co-administered drugs.

TABLE 4.43: Metabolic Properties Comparison

Reference Drug	**Imiquiomod**	**Magnoflorine**	**Thalifendine**
CYP2D6 substrate	No	No	No
CYP3A4 substrate	No	Yes	Yes
CYP1A2 inhibitor	Yes	Yes	Yes
CYP2C19 inhibitor	Yes	No	No
CYP2C9 inhibitor	No	No	No
CYP2D6 inhibitor	No	No	Yes
CYP3A4 inhibitor	No	No	No

4.15.16 Distribution Properties Comparison

Distribution properties determine the efficiency of a drug to arrive at its target tissues and organs. One key parameter is the volume of distribution at steady state (VDss), which predicts the level at which a chemical substance spreads from the bloodstream into tissues. In silico predictions indicated that Imiquimod exhibits a moderate VDss, reflecting a balanced distribution between plasma and tissue compartments. Similarly, Magnoflorine and Thalifendine showed comparable VDss values, suggesting adequate systemic distribution. Another critical factor is blood-brain barrier (BBB) permeability. Imiquimod was predicted to have low BBB permeability, which is consistent with its peripheral site of action. Magnoflorine and Thalifendine also exhibited low BBB permeability, reducing the risk of central nervous system side effects. All three compounds demonstrated plasma protein binding (PPB) within a normal range, supporting good bioavailability and minimal sequestration in blood plasma. These properties highlight the favorable distribution behavior of the selected plant compounds in comparison to the reference drug.

TABLE 4.44: Comparison of distribution characteristics

Standard Drug	**Imiquiomod**	**Magnoflorine**	**Thalifendine**
VDss (human)	0.736	1.211	0.993

Table 4.44 continued from previous page

Standard Drug	Imiquiomod	Magnoflorine	Thalifendine
Fraction unbound (human)	0.141	0.105	0.239
BBB Permeability	0.212	-0.651	0.147
CNS Permeability	-2.051	-2.101	-2.037

4.15.17 Excretion Properties Comparison

Excretion properties are crucial for understanding the elimination pathway and clearance rate of drug candidates from the body. In silico analysis predicted that all three compounds — Imiquimod, Magnoflorine, and Thalifendine — exhibit moderate total clearance rates, suggesting a balanced elimination through hepatic and renal pathways.None of the compounds showed renal properties cation transporter 2 (OCT2) substrates, which indicates a reduced risk of renal accumulation or nephrotoxicity. The moderate clearance rates suggest that these compounds can maintain therapeutic levels without rapid elimination or prolonged retention, which is favorable for dose regulation. These results show that the excretion profiles of Magnoflorine and Thalifendine are consistent with that of the clinically approved drug Imiquimod, further supporting their suitability as lead candidates.

Table 4.45: Excretion Properties Comparsion

Standard Drug	Imiquiomod	Magnoflorine	Thalifendine
Total Clearance	0.79	1.083	1.244
Renal OCT2 Substrate	Yes	No	No

4.15.18 Docking Score Comparison

Docking analysis was performed on both standard and lead compounds against *E6* and *E7* to identify the compound with the highest binding affinity.

Table 4.46: Docking Score Comparison Against Protein E6

S.No	Compound	Bindng Score
1	Imiquiomod	-6.5

Table 4.46 continued from previous page

S.No	Compound	Bindng Score
2	Magnoflorine	-7.1
3	Thalifendine	-6.7

TABLE 4.47: Docking Score Comparison Against Protein E7

S.No	Compound	Bindng Score
1	Imiquiomod	-6.0
2	Magnoflorine	-6.3
3	Thalifendine	-7.1

4.15.19 Docking Analysis Comparison

LigPlot analyzes the docking results by evaluating the number of hydrogen bonds, hydrophobic interactions, interacting amino acids, and steric interactions.

Figure 4.37 shows the association of Imiquimod with protein *E6*. It shows that imiquimod has formed Twelve hydrophobic interactions.

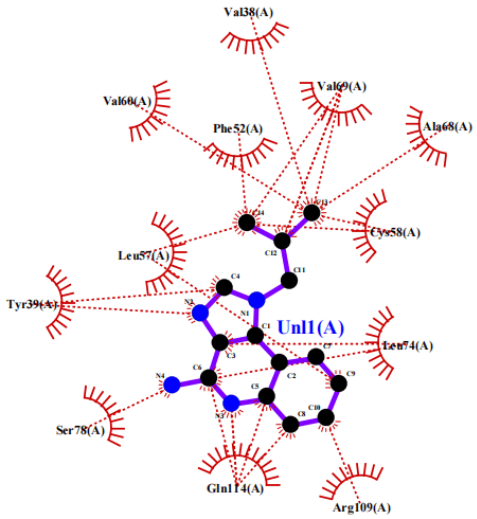

FIGURE 4.37: Interaction of Imiquimod with receptor protein *E6*

Figure 4.38 shows the interaction of Imiquimod with receptor protein *E7*. It shows that imiquimod has formed eight hydrophobic interactions and Two hydrogen bond.

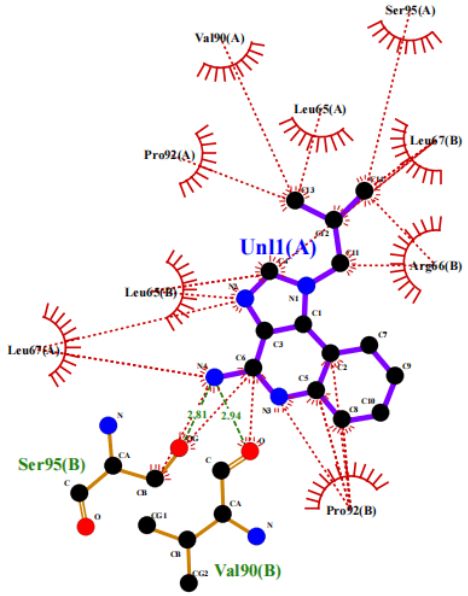

FIGURE 4.38: Interaction of Imiquimod with receptor protein *E7*

Figure 4.39 shows the interaction of Magnoflorine with receptor protein *E6*. It shows that Magnoflorine has formed eight hydrophobic interactions and Three hydrogen bond.

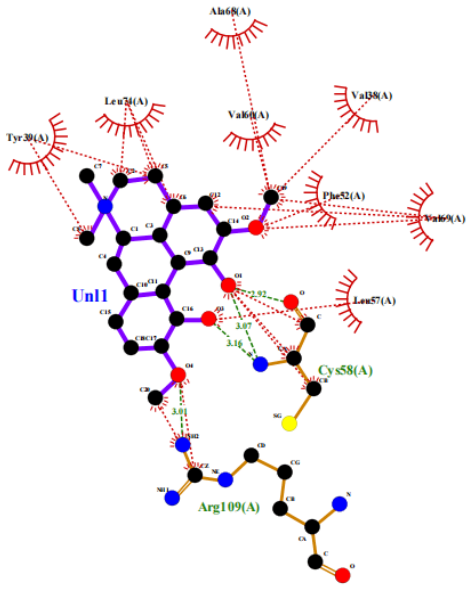

FIGURE 4.39: Interaction of Magnoflorine with receptor protein *E6*

Figure 4.40 shows the interaction of Magnoflorine with receptor protein *E7*. It shows that Magnoflorine has formed eight hydrophobic interactions and one hydrogen bond.

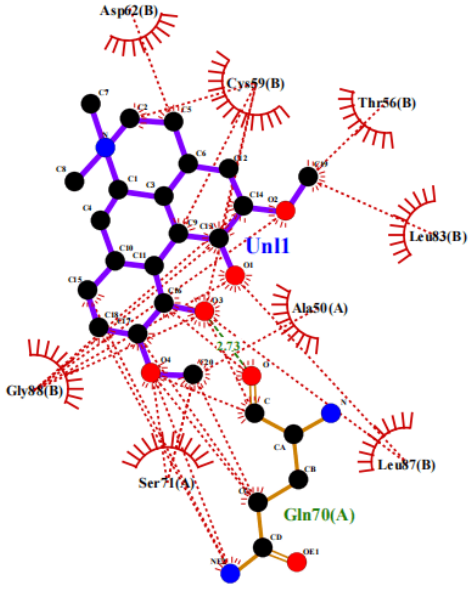

FIGURE 4.40: Interaction of Magnoflorine with receptor protein *E7*

Figure 4.41 shows the interaction of Thalifendine with receptor protein *E6*. It shows that Thalifendine has formed Five hydrophobic interactions and one hydrogen bond.

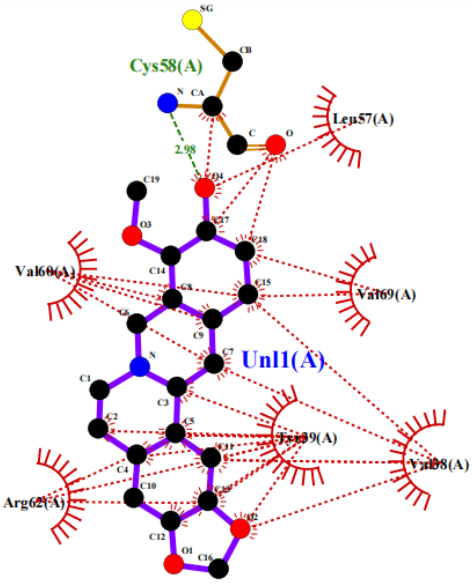

FIGURE 4.41: Interaction of Thalifendine with receptor protein *E6*

Figure 4.42 shows the interaction of Thalifendine with receptor protein *E7*. It shows that Thalifendine has formed Twelve hydrophobic interactions and one hydrogen bond.

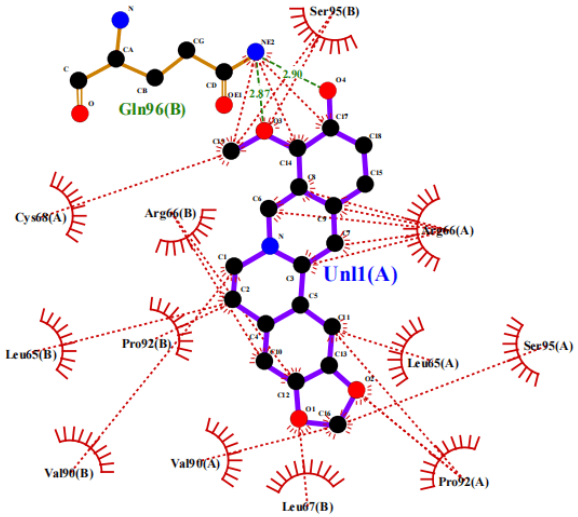

FIGURE 4.42: Interaction of Thalifendine with receptor protein *E7*

Chapter 5

Conclusions and Recommendations

The present study was aimed at the identification of potential antiviral agents from *Berberis vulgaris* targeting oncoproteins *E6* and *E7* from Human Papillomavirus type 16 using a comprehensive *in silico* approach. A total of selected phytochemicals were evaluated through molecular docking, ADME analysis, and toxicity prediction. Among them, **Magnoflorine** and **Thalifendine** emerged as promising lead compounds due to their strong binding affinities with *E6* and *E7* proteins, respectively, along with excellent drug-likeness profiles. Both compounds showed high gastrointestinal absorption, no predicted toxicity, non-inhibition of major CYP450 enzymes, and moderate clearance, indicating overall pharmacokinetic stability. In comparison to the clinically approved drug Imiquimod, which exhibited lower binding scores and possible localized side effects, these plant-derived alkaloids displayed superior interaction profiles and safety predictions. These findings support the hypothesis that natural compounds from *Berberis vulgaris* hold potential as effective antiviral agents against HPV16 and warrant further experimental validation.

5.1 Recommendation:

In vitro validation of Magnoflorine and Thalifendine should be conducted using HPV16-infected cell lines to assess their biological activity. In vivo studies are recommended to evaluate the pharmacokinetic behavior, bioavailability, and toxicity in animal models. Structural optimization and semi-synthetic derivatives of these compounds can be explored to enhance target specificity and potency .Future studies should incorporate molecular dynamics simulations to evaluate the long-term stability of the protein-ligand complex.. Additional bioactive compounds from *Berberis vulgaris* and other medicinal plants should be screened to expand the pool of potential anti-HPV agents.

Bibliography

[1] E. V. Koonin *et al.*, "Evolution of viruses and related mobile genetic elements," *Microbial Biol Rev*, vol. 79, no. 1, pp. 1–25, 2015.

[2] C. de Martel *et al.*, "Global burden of cancers attributable to infections," *Int J Cancer*, vol. 147, no. 3, pp. 691–700, 2020.

[3] D. Bzhalava *et al.*, "Papillomavirus typing," *Clin Microbiol Infect*, vol. 19, no. 1, pp. 10–14, 2013.

[4] G. M. Clifford *et al.*, "Human papillomavirus types in invasive cervical cancer worldwide: a meta-analysis," *Br J Cancer*, vol. 88, no. 1, pp. 63–73, 2003.

[5] D. Forman *et al.*, "Global burden of human papillomavirus and related diseases," *Vaccine*, vol. 30, no. Suppl 5, pp. F12–F23, 2012.

[6] K. Münger *et al.*, "Mechanisms of human papillomavirus-induced oncogenesis," *J Virol*, vol. 78, no. 21, pp. 11 451–11 460, 2004.

[7] J. Doorbar *et al.*, "The biology and life-cycle of human papillomaviruses," *Vaccine*, vol. 30, no. Suppl 5, pp. F55–F70, 2012.

[8] V. Tomaić, "Functional roles of e6 and e7 oncoproteins in hpv-induced malignancies at diverse anatomical sites," *Cancerss*, vol. 8, no. 10, p. 95, 2016.

[9] D. J. Newman and G. M. Cragg, "Natural products as sources of new drugs," *J Nat Prod*, vol. 83, no. 3, pp. 770–803, 2020.

[10] M. Imenshahidi and H. Hosseinzadeh, "Berberis vulgaris and berberine: An update review," *Phytother Res*, vol. 30, no. 11, pp. 1745–1764, 2016.

[11] D. B. Kitchen *et al.*, "Docking and scoring in virtual screening for drug discovery: methods and applications," *Nat Rev Drug Discov*, vol. 3, no. 11, pp. 935–949, 2004.

[12] X. Y. Meng *et al.*, "Molecular docking: a powerful approach for structure-based drug discovery," *Curr Comput Aided Drug Des*, vol. 7, no. 2, pp. 146–157, 2011.

[13] E. V. Koonin *et al.*, "Evolution of viruses and related mobile genetic elements," *Microbiol Mol Biol Rev*, vol. 79, no. 1, pp. 1–25, 2015.

[14] E. M. de Villiers, "Cross-roads in the classification of papillomaviruses," *Virology*, vol. 445, no. 1-2, pp. 2–10, 2013.

[15] D. Bzhalava *et al.*, "Papillomavirus typing," *Clin Microbiol Infect*, vol. 19, no. 1, pp. 10–14, 2013.

[16] G. M. Clifford *et al.*, "Human papillomavirus types in invasive cervical cancer worldwide: a meta-analysis," *Br J Cancer*, vol. 88, no. 1, pp. 63–73, 2003.

[17] D. Forman *et al.*, "Global burden of human papillomavirus and related diseases," *Vaccine*, vol. 30, no. Suppl 5, pp. F12–F23, 2012.

[18] K. Münger *et al.*, "Mechanisms of human papillomavirus-induced oncogenesis," *J Virol*, vol. 78, no. 21, pp. 11 451–11 460, 2004.

[19] C. A. Moody and L. A. Laimins, "Human papillomavirus oncoproteins: pathways to transformation," *Nat Rev Cancer*, vol. 10, no. 8, pp. 550–560, 2010.

[20] I. G. Bravo and M. Félez-Sánchez, "Papillomaviruses: Viral evolution, cancer and evolutionary medicine," *Evol Med Public Health*, vol. 2015, no. 1, pp. 32–51, 2015.

[21] K. V. Doorslaer *et al.*, "The papillomavirus episteme: a major update to the papillomavirus sequence database," *Nucleic Acids Res*, vol. 45, no. D1, pp. D499–D506, 2017.

[22] H. U. Bernard *et al.*, "Classification of papillomaviruses (pvs) based on 189 pv types and proposal of taxonomic amendments," *Virology*, vol. 401, no. 1, pp. 70–79, 2010.

[23] M. Gottschling *et al.*

[24] S. V. Graham, "Papillomavirus entry, infection, and tropism," *Virology*, vol. 445, no. 1-2, pp. 115–122, 2017.

[25] J. T. Schiller, P. M. Day, and R. C. Kines, "Current understanding of the mechanism of hpv infection," *Gynecol Oncol*, vol. 118, no. 1 Suppl, pp. S12–S17, 2010.

[26] A. B. Raff *et al.*, "The evolving field of human papillomavirus receptor research: a review of binding and entry," *J Virol*, vol. 87, no. 11, pp. 6062–6072, 2013.

[27] G. Spoden *et al.*, "Clathrin- and caveolin-independent entry of human papillomavirus type 16—involvement of tetraspanin-enriched microdomains (tems)," *PLoS One*, vol. 3, no. 10, p. e3313, 2008.

[28] S. DiGiuseppe *et al.*, "The minor capsid protein l2 enhances hpv16 l1 pseudovirion stability," *J Virol*, vol. 88, no. 10, pp. 6149–6158, 2014.

[29] D. Pyeon, S. M. Pearce, S. M. Lank, P. Ahlquist, and P. F. Lambert, "Establishment of human papillomavirus infection requires cell cycle progression," *PLoS Pathog*, vol. 5, no. 2, p. e1000318, 2009.

[30] A. A. McBride, "The papillomavirus e2 proteins," *Virology*, vol. 445, no. 1-2, pp. 57–79, 2013.

[31] S. V. Graham, "Keratinocyte differentiation-dependent human papillomavirus gene regulation," *Viruses*, vol. 9, no. 9, p. 245, 2017.

[32] J. Doorbar, "The papillomavirus life cycle," *J Clin Virol*, vol. 32, no. Suppl 1, pp. S7–S15, 2005.

[33] C. P. Crum and G. J. Nuovo, "The natural history of hpv infection and its link to cervical cancer: Cytologic and histologic aspects," *Obstet Gynecol Clin North Am*, vol. 23, no. 3, pp. 655–673, 1996.

[34] M. Stanley, "Immune responses to human papillomavirus," *Vaccine*, vol. 24, no. Suppl 1, pp. S16–S22, 2006.

[35] A. B. Moscicki, "Natural history of hpv infection," *J Adolesc Health*, vol. 43, no. 4 Suppl, pp. S3–S9, 2008.

[36] N. Munoz *et al.*, "Epidemiologic classification of human papillomavirus types associated with cervical cancer," *N Engl J Med*, vol. 348, no. 6, pp. 518–527, 2003.

[37] S. M. Garland *et al.*, "Quadrivalent vaccine against human papillomavirus to prevent anogenital diseases," *N Engl J Med*, vol. 356, no. 19, pp. 1928–1943, 2007.

[38] F. X. Bosch *et al.*, "The causal relation between human papillomavirus and cervical cancer," *J Clin Pathol*, vol. 55, no. 4, pp. 244–265, 2002.

[39] M. Schiffman *et al.*, "Human papillomavirus and cervical cancer," *Lancet*, vol. 370, no. 9590, pp. 890–907, 2007.

[40] E. J. Crosbie, M. H. Einstein, S. Franceschi, and H. C. Kitchener, "Human papillomavirus and cervical cancer," *Lancet*, vol. 382, no. 9895, pp. 889–899, 2013.

[41] M. L. Gillison *et al.*, "Evidence for a causal association between human papillomavirus and a subset of head and neck cancers," *J Natl Cancer Inst*, vol. 92, no. 9, pp. 709–720, 2000.

[42] C. S. Derkay and B. Wiatrak, "Recurrent respiratory papillomatosis: a review," *Laryngoscope*, vol. 118, no. 7, pp. 1236–1247, 2008.

[43] M. Arbyn *et al.*, "European guidelines for quality assurance in cervical cancer screening: recommendations for hpv testing," *Eur J Cancer*, vol. 46, no. 3, pp. 312–320, 2010.

[44] WHO/ICO Information Centre on HPV and Cervical Cancer, "Pakistan report," World Health Organization, Tech. Rep., 2023.

[45] C. de Martel *et al.*, "Global burden of cancers attributable to infections," *Int J Cancer*, vol. 147, no. 3, pp. 691–700, 2020.

[46] M. F. Nasir *et al.*, "Human papillomavirus genotype distribution in invasive cervical cancer in pakistan," *Cancers*, vol. 8, no. 8, p. 72, 2016.

[47] N. Gul *et al.*, "Hpv detection in cervical cancer samples from islamabad and rawalpindi," *Int J Infect Dis*, 2015.

[48] N. Siddiqa *et al.*, "Prevalence and genotype distribution of high-risk hpv in punjab," *Viruses*, vol. 6, no. 7, p. 2762, 2014.

[49] Z. Basharat *et al.*, "Hpv awareness and vaccination barriers in pakistan," *JCO Glob Oncol*, 2024.

[50] World Health Organization, "Global strategy to accelerate the elimination of cervical cancer," World Health Organization, Tech. Rep., 2021.

[51] D. J. Wiley *et al.*, "External genital warts: diagnosis, treatment, and prevention," *Clin Infect Dis*, vol. 35, no. Suppl 2, pp. S210–S224, 2002.

[52] L. S. Massad *et al.*, "2012 updated consensus guidelines for the management of abnormal cervical cancer screening tests and cancer precursors," *J Low Genit Tract Dis*, vol. 17, no. 5 Suppl 1, pp. S1–S27, 2013.

[53] C. L. Trimble *et al.*, "Safety, efficacy, and immunogenicity of vgx-3100, a therapeutic synthetic dna vaccine targeting hpv16 and 18 e6 and e7 proteins for cervical intraepithelial neoplasia 2/3: a randomised, double-blind, placebo-controlled phase 2b trial," *Lancet*, vol. 386, no. 10008, pp. 2078–2088, 2015.

[54] D. J. Newman and G. M. Cragg, "Natural products as sources of new drugs over the nearly four decades from 01/1981 to 09/2019," *J Nat Prod*, vol. 83, no. 3, pp. 770–803, 2020.

[55] S. M. K. Rates, "Plants as source of drugs," *Toxicon*, vol. 39, no. 5, pp. 603–613, 2001.

[56] M. Imenshahidi and H. Hosseinzadeh, "Berberis vulgaris and berberine: An update review," *Phytother Res*, vol. 30, no. 11, pp. 1745–1764, 2016.

[57] J. Kim, K. J. Lee, J. H. Kim *et al.*, "Berberine inhibits human papillomavirus oncogene expression by suppressing ap-1 and nf-ϰb in cervical cancer cells," *Int J Oncol*, vol. 43, no. 6, pp. 1799–1806, 2013.

[58] X. Liu, Q. Ji, N. Ye *et al.*, "Berberine inhibits hpv oncogene transcription by downregulating e6/e7 promoter activity and histone acetylation," *Mol Med Rep*, vol. 13, no. 6, pp. 5237–5245, 2016.

[59] D. M. Maher, M. C. Bell, E. A. O'Donnell *et al.*, "Curcumin suppresses human papillomavirus oncoproteins by restoring tumor suppressor pathways in hpv-positive head and neck cancer cells," *Int J Oncol*, vol. 39, no. 2, pp. 521–528, 2011.

[60] Z. Y. Wang, N. Wang, S. B. Han *et al.*, "Natural products in the prevention and treatment of cervical cancer: a review," *Molecules*, vol. 24, no. 17, p. 3169, 2019.

[61] E. Gulletta *et al.*, "Phytochemicals targeting human papillomavirus infection and associated cancers: A review," *Curr Drug Targets*, vol. 22, no. 10, pp. 1073–1084, 2021.

[62] M. Imenshahidi and H. Hosseinzadeh, "Berberis vulgaris and berberine: An update review," *Phytother Res*, vol. 30, no. 11, pp. 1745–1764, 2016.

[63] J. Kim, K. J. Lee, J. H. Kim *et al.*, "Berberine inhibits human papillomavirus oncogene expression by suppressing ap-1 and nf-ϰb in cervical cancer cells," *Int J Oncol*, vol. 43, no. 6, pp. 1799–1806, 2013.

[64] X. Liu, Q. Ji, N. Ye *et al.*, "Berberine inhibits hpv oncogene transcription by downregulating e6/e7 promoter activity and histone acetylation," *Mol Med Rep*, vol. 13, no. 6, pp. 5237–5245, 2016.

[65] D. M. Maher, M. C. Bell, E. A. O'Donnell *et al.*, "Curcumin suppresses human papillomavirus oncoproteins by restoring tumor suppressor pathways

in hpv-positive head and neck cancer cells," *Int J Oncol*, vol. 39, no. 2, pp. 521–528, 2011.

[66] Y. Wu, W. Li, Y. Xu *et al.*, "Berberine inhibits cervical cancer cell growth by inducing g1-phase cell cycle arrest and apoptosis via suppression of pi3k/akt pathway," *J Cell Biochem*, vol. 120, no. 3, pp. 4299–4310, 2019.

[67] K. Wang, X. Feng, L. Chai, S. Cao, and F. Qiu, "The anti-tumor activities of natural product berberine against human cervical cancer cells are associated with suppression of hpv oncogenes and inflammation-related signaling pathways," *Phytomedicine*, vol. 21, no. 6, pp. 855–860, 2014.

[68] X. Liu, X. Zhang, L. Wang *et al.*, "Berberine targets epigenetic modification to suppress hpv oncogene expression in cervical cancer cells," *Biomed Pharmacother*, vol. 104, pp. 715–721, 2018.

[69] J. J. Lu, J. L. Bao, X. P. Chen, M. Q. Huang, and Y. T. Wang, "Alkaloids isolated from natural herbs as the anticancer agents," *Evid Based Complement Alternat Med*, vol. 2012, p. 485042, 2012.

[70] Z. Wang, N. Wang, S. Han, D. Wang, S. Mo, and L. Yu, "Berberine and its derivatives as potential agents for the treatment of hpv-related cervical cancer," *Front Pharmacol*, vol. 12, p. 660093, 2021.

[71] X. Y. Meng *et al.*, "Molecular docking: a powerful approach for structure-based drug discovery," *Curr Comput Aided Drug Des*, vol. 7, no. 2, pp. 146–157, 2011.

[72] D. B. Kitchen *et al.*, "Docking and scoring in virtual screening for drug discovery: methods and applications," *Nat Rev Drug Discov*, vol. 3, no. 11, pp. 935–949, 2004.

[73] G. M. Morris and M. Lim-Wilby, "Molecular docking," in *Molecular Modeling of Proteins*. Springer, 2008, pp. 365–382.

[74] N. S. Pagadala, K. Syed, and J. Tuszynski, "Software for molecular docking: a review," *Biophys Rev*, vol. 9, no. 2, pp. 91–102, 2017.

[75] L. G. Ferreira, R. N. D. Santos, G. Oliva, and A. D. Andricopulo, "Molecular docking and structure-based drug design strategies," *Molecules*, vol. 20, no. 7, pp. 13 384–13 421, 2015.

[76] T. Lengauer and M. Rarey, "Computational methods for biomolecular docking," *Curr Opin Struct Biol*, vol. 6, no. 3, pp. 402–406, 1996.

[77] E. Lionta, G. Spyrou, D. K. Vassilatis, and Z. Cournia, "Structure-based virtual screening for drug discovery: principles, applications and recent advances," *Curr Top Med Chem*, vol. 14, no. 16, pp. 1923–1938, 2014.

[78] B. K. Shoichet, "Virtual screening of chemical libraries," *Nature*, vol. 432, no. 7019, pp. 862–865, 2004.

[79] E. Yuriev and P. A. Ramsland, "Latest developments in molecular docking: 2010–2011 in review," *J Mol Recognit*, vol. 26, no. 5, pp. 215–239, 2013.

[80] D. J. Newman and G. M. Cragg, "Natural products as sources of new drugs over the nearly four decades from 01/1981 to 09/2019," *J Nat Prod*, vol. 83, no. 3, pp. 770–803, 2020.

[81] J. Kim, K. J. Lee, J. H. Kim *et al.*, "Berberine inhibits human papillomavirus oncogene expression by suppressing ap-1 and nf-ϰb in cervical cancer cells," *Int J Oncol*, vol. 43, no. 6, pp. 1799–1806, 2013.

[82] J. Doorbar *et al.*, "The biology and life-cycle of human papillomaviruses," *Vaccine*, vol. 30, no. Suppl 5, pp. F55–F70, 2012.

[83] J. Kim, K. J. Lee, J. H. Kim *et al.*, "Berberine inhibits human papillomavirus oncogene expression by suppressing ap-1 and nf-ϰb in cervical cancer cells," *Int J Oncol*, vol. 43, no. 6, pp. 1799–1806, 2013.

[84] D. N. Sauder, "Imiquimod: mode of action," *Br J Dermatol*, vol. 149, no. Suppl 66, pp. 5–8, 2003.

[85] N. Kumar, R. Tomar, A. Pandey, V. Tomar, V. K. Singh, and R. Chandra, "Preclinical evaluation and molecular docking of 1, 3-benzodioxole propargyl ether derivatives as novel inhibitor for combating the histone deacetylase

enzyme in cancer," *Artif Cells Nanomed Biotechnol*, vol. 46, no. 6, pp. 1288–1299, 2018.

[86] A. Daina, O. Michielin, and V. Zoete, "Swissadme: a free web tool to evaluate pharmacokinetics, drug-likeness and medicinal chemistry friendliness of small molecules," *Sci Rep*, vol. 7, no. 1, pp. 1–13, 2017.

[87] C. A. Lipinski, "Lead-and drug-like compounds: the rule-of-five revolution," *Drug Discov Today Technol*, vol. 1, no. 4, pp. 337–341, 2004.